AD-A087 672 OXFORD UNIV (ENGLAND) DEPT OF THEORETICAL CHEMISTRY F/G 7/2
INTERATOMIC FORCES IN SOLID AND LIQUID TRANSITION METALS.(U)
JAN 80 N H MARCH, C C MATTHAI, P J GROUT DA-ERO-78-G-052

UNCLASSIFIED NL

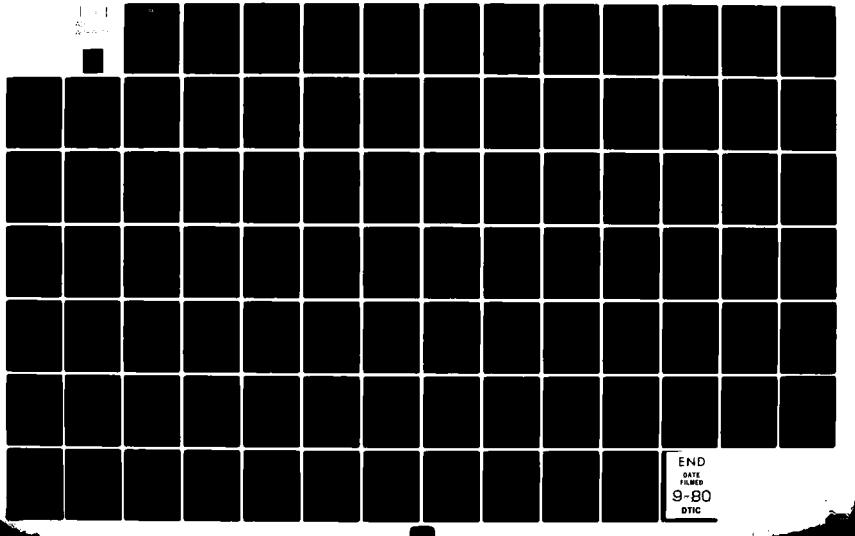

END
DATE FILMED
9-80
DTIC

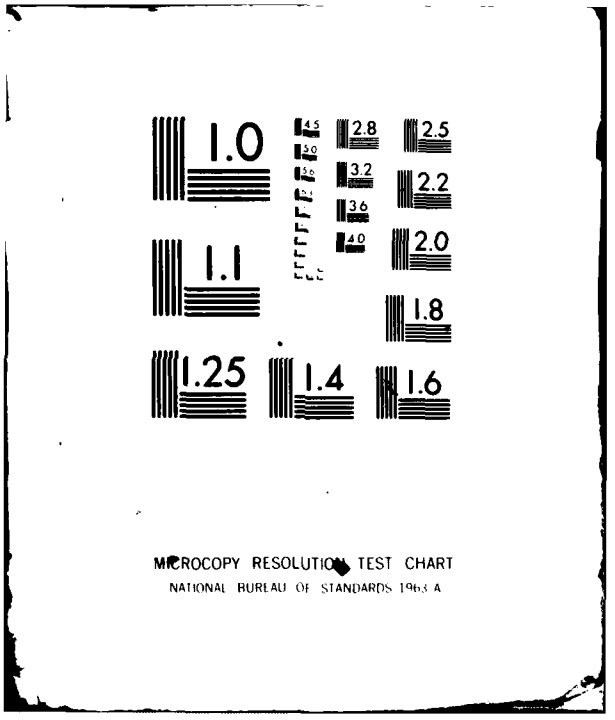
1.0
1.1
1.25
1.4
1.6
1.8
2.0
2.2
2.5
2.8
3.2
3.6
4.0
4.5
5.0
MICROCOPY RESOLUTION TEST CHART
NATIONAL BUREAU OF STANDARDS 1963 A

Interatomic Forces in Solid and Liquid Transition Metals

Final Technical Report

by

N.H. March, C.C. Matthai and P.J. Grout

January 1980

EUROPEAN RESEARCH OFFICE
United States Army
London England

GRANT NUMBER DA-ERO - 78 - G - 052

Oxford University (Theoretical Chemistry Department)

UNCLASSIFIED

SECURITY CLASSIFICATION OF THIS PAGE (When Date Entered)

R&D 2286A

REPORT DOCUMENTATION PAGE

READ INSTRUCTIONS BEFORE COMPLETING FORM

1. REPORT NUMBER

2. GOVT ACCESSION NO. AD-A087672

3. RECIPIENT'S CATALOG NUMBER

4. TITLE (and Subtitle)

(6) Interatomic Forces in Solid and Liquid Transition Metals.

5. TYPE OF REPORT & PERIOD COVERED
Final Tech. Report
Apr 78 - Mar 80

6. PERFORMING ORG. REPORT NUMBER

7. AUTHOR(a)

(10) N.H. March, C.C. Matthai [redacted] P.J. Grout

8. CONTRACT OR GRANT NUMBER(a)

(15) DAER078-G-0052

9. PERFORMING ORGANIZATION NAME AND ADDRESS

U. of Oxford
Oxford UK

10. PROGRAM ELEMENT, PROJECT, TASK AREA & WORK UNIT NUMBERS

6.11.02A 1T161102BH57-07

(16) (17)

11. CONTROLLING OFFICE NAME AND ADDRESS

USARDSG-UK
Box 65
NY 09510

(12) 93 (11)

12. REPORT DATE
Jan [redacted] 80

13. NUMBER OF PAGES
87

14. MONITORING AGENCY NAME & ADDRESS(if different from Controlling Office)

15. SECURITY CLASS. (of this report)
UNCLASSIFIED

15a. DECLASSIFICATION/DOWNGRADING SCHEDULE

16. DISTRIBUTION STATEMENT (of this Report)

Approved for Public Release; Distribution Unlimited

(14) Final Tech. Rept. Apr 78 - Mar 80

17. DISTRIBUTION STATEMENT (of the abstract entered in Block 20, if different from Report)

18. SUPPLEMENTARY NOTES

19. KEY WORDS (Continue on reverse side if necessary and identify by block number)

Transition metals, interatomic forces, X-ray scattering, Wannier functions, pair potentials.

20. ABSTRACT (Continue on reverse side if necessary and identify by block number)

(19) The objective was to obtain a practical description of the force fields in transition metals. Central pair potentials for Ni and Pt have been constructed in agreement with calculations and experiments. The obtained representation of the force field is very useful for f.c.c. solid transition metals. X-ray scattering factors showed that charge distribution in b.c.c. transition metals is highly angular. Bond charge model has been used to represent this angularity.

DD FORM 1 JAN 73 1473 EDITION OF 1 NOV 65 IS OBSOLETE

UNCLASSIFIED

SECURITY CLASSIFICATION OF THIS PAGE (When Date Entered)

4/11/85

Abstract

INTERATOMIC FORCES IN TRANSITION METALS

In this work we have been concerned with obtaining a practical description of the force fields in transition metals. There is some evidence that directional effects due to the d orbitals of the transition metals increase through the sequence face centred cubic (f.c.c.), hexagonal close packed (h.c.p.) and body centred cubic (b.c.c.) structures. These features have led us to study the utility of density-independent central pair forces, plus a volume-dependent energy for the f.c.c. metals Ni and Pt. We have constructed central pair potentials for both these metals which give fair agreement between the calculated and experimentally determined phonon dispersion curves and liquid structure factors. While the above results strongly demonstrate the usefulness of such a representation of the force fields in the f.c.c. solid transition metals, we have, by studying the X-ray scattering factors, found the charge distribution in the b.c.c. transition metals to be highly angular. Using a Wannier function formalism, we have found that this angularity can be well represented by a bond charge model in which the bond charges are situated at nearest and next nearest neighbour interstitials. The angularity in the charge distribution is a result of degenerate bands forming hybrid wavefunctions. In h.c.p. Be the degenerate bands lead to sp hybridization. The usefulness of the Wannier formalism was investigated quantitatively by calculating the X-ray scattering factors of Be. Expressions for the elastic constants and phonon dispersion relations have been derived for this bond charge model and used to calculate these properties of Fe. The fair agreement with the experimentally determined phonon dispersion curves shows that in addition to the central ion-ion pair interactions, there also exists bond electron-ion and bond electron-bond electron pair interactions in the transition metals.

Table of Contents

CHAPTER 1

Introduction

Any real understanding of the physics of metals must entail some knowledge of the force fields. Since the force fields are determined by the interaction of the ions and electrons amongst themselves, an accurate knowledge of the force fields can be obtained if the electronic distribution is known. Thus, we may determine the force fields either directly, by analysing experimental data (e.g. the phonon dispersion data) or indirectly, by building a picture of the charge density in the metal.

The pseudopotential theory of metals which makes use of the free electron model allows one to write the total energy of a crystal in terms of the dielectric function, which describes the electronic distribution. For a free electron gas, and working to second order in the perturbing electron-ion interaction, it turns out that this may be further simplified into a sum of effective ion-ion central pair interactions and a volume dependent structure independent energy. Since this theory has proved quite successful for the simple metals, it implies that the force fields in these metals can be represented by central pair ion-ion interactions.

Harrison (1969) extended this model for the d-band metals by including in the total wavefunction d-resonance states to account for the unfilled d-band, and also a hybridization term. Using this model, Moriarty (1972) was able to determine effective interionic potentials in the noble metals by working to second order in the perturbation. Although hybridization was included, the pair interactions were taken to be central. This approach is inconsistent with the angularity present in the charge density due to hybridization.

Bertoni et al. (1975) calculated the phonon dispersion curves and elastic constants of Be and found that an exten-

sion of the pseudopotential theory to third order was needed to obtain reasonable agreement with experiment. Since this extension yields not only pair forces, but also three body forces, it is indicative of the non-central nature of the force fields. It is interesting to note that the main feature common to Be and the d-band metals is that of overlapping valence bands. It, therefore, appears that; unlike in the simple metals, the force fields in crystals with degenerate bands are non-central. In this work, we have addressed ourselves to two questions:

(i) Although the force fields in the d-band metals will undoubtedly be non-central, can the approximation of central forces in some d-band metals still be a useful one.

(ii) In these d-band metals where the central approximation fails, how can the non-central character of the forces be usefully represented.

A first principles calculation of the force field in a metal requires knowledge of the dielectric function of the electron distribution. As even in the simple metals the uncertainty in the dielectric function leads to widely varying interatomic potentials (Ashcroft and Langreth 1967, Ho 1970) there is little hope of obtaining a good potential for any of the transition metals. We have adopted, therefore, a procedure which is semiempirical, but in which the essential guidelines laid down by the electron theory of d-band metals are taken into account as follows:

(i) The intermediate and long range interactions are oscillatory in nature and have the form $\cos(ar+b)/r^3$.

(ii) The d-shells lead to considerably harder repulsive core-core interactions than in the simple sp metals.

(iii) The directional effects due to the d-electrons appear to vary according to the structure of the crystalline transition metals. If one adopts an approach based on hybrids of d orbitals with s and p orbitals, then the crystal symmetry indicates which are the appropriate hybrids.

These guidelines have been taken into account in our work, in an admittedly incomplete way, as follows:

(a) It is a well-known fact that the volume change of a metal upon melting is sufficiently small to allow one to extract information on the interatomic forces in the solid from the liquid state. In a classical liquid, the structure factor is directly related to the effective interaction potential. As the measured liquid structure factors of the d-band metals do not differ qualitatively from those of the simple metals (Huijben and van der Lugt 1979, Waseda and Ohtani 1974), we have assumed that in the liquid state the force fields are also qualitatively the same.

(b) From liquid metal data interpreted on the basis of pair interactions, we have been able to extrapolate approximate interatomic pair potentials at near equilibrium distances.

(c) Both liquid structure and radiation damage data have been used to obtain an estimate of core hardness. Also, the melting curves of the d-band metals under pressure lends support to our estimates of core repulsion.

(d) From the crystal structure, using group theoretical techniques, appropriate hybrids have been constructed and the resulting charge distribution modelled by bond charges.

Having obtained suitable representations for the charge distribution and force fields in particular d-band metals, we have proceeded to test their usefulness by examining their effects on the second and third-order elastic constants by studying the phonon dispersion curves and by investigating the single crystal X-ray scattering experiments.

In Chapter 2 we, by representing the force fields in the face centred cubic (f.c.c.) d-band metals by central pair interactions, calculate pair potentials for Ni and Pt using liquid structure and phonon dispersion data (Matthai et al. 1978a).

The angularity in the charge distribution in the transition metals is discussed in Chapter 3, and a formalism for the X-ray scattering factors in solids, in terms of Wannier functions is set up (Matthai et al. 1978b). With this formalism, the measurements of the body centred cubic (b.c.c.) transition metals are explained. Since a quantitative explanation requires us to know the Wannier functions, we, by calculating them approximately, have determined the X-ray scattering factors of Be. This is presented in Chapter 4.

In Chapter 5, by means of a model the angularity of the charge distribution is incorporated into the force fields. This enables us to calculate the phonon dispersion curves of Fe. Finally, the accuracy of the potentials presented in this work are discussed, and ways to improve them are suggested in Chapter 6.

CHAPTER 2

Pair potentials in the f.c.c. transition metals

§2.1 Introduction

If we consider a metal to be a collection of ions positioned at lattice sites surrounded by some inhomogeneous electron distribution, then, we can write the total energy, E, of the metal as

$$E = E_C + E_A + E_V \tag{2.1}$$

where $E_C + E_V$ is that part arising from only considering the spatially homogeneous part of the electron distribution and E_A is the extra energy arising from the spatial inhomogeniety. From experimental evidences about the charge density distributions, it appears that the charge distributions of the f.c.c. transition metals are more homogeneous than that of the b.c.c. metals. We have therefore made the approximation that E_A may be neglected for the f.c.c. metals and thus can be treated like a simple metal (sp).

In the simple metals the model can be simplified to one of spherically symmetric charged ions situated at lattice sites immersed in a homogeneous electron gas. Thus the ions interact between themselves directly and indirectly via the electron gas. The contribution to the energy from the direct ion-ion interaction consists of the direct coulomb repulsion between the ions, and the energy arising from the repulsion due to the overlap of the ion cores, E_R. In the theory of the simple metals, it can be shown (Harrison 1966) that the direct coulomb repulsion together with the screened interaction gives rise to a contribution to the total energy of $E_P + E_V$, where

$$E_P = \sum_{ij} \phi(r_{ij}) \tag{2.2};$$

$$\phi(r) = \frac{B}{r^3} \cos 2k_F r \tag{2.3},$$

E_V is a volume dependent structure independent energy and k_F is the Fermi wavevector.

The change in energy in bringing two ions from infinity to a separation R, ΔE, can be shown to be (Dick and Overhauser 1958)

$$\Delta E = \frac{e q_{ex}}{2R} \quad ; \quad q_{ex} = 4S^2 \tag{2.4}$$

where S is the overlap integral. Since this energy is positive, there is overall repulsion between the atoms. Over the range under consideration, this change in energy can also be fitted by the Born-Mayer (B-M) form, $\exp(-R/R_o)$ and for more complex shelled ions we expect the same form for the repulsive energy, namely

$$\Delta E = \frac{\gamma q_{ex}}{R} = A \exp(-bR) \tag{2.5}$$

where γ, A and b are constants.

In the rare gas solids, the core-core repulsion is often characterised by an inverse power potential, as in the case of the Lennard-Jones potential.

The repulsive potential expressed either in the B-M or inverse power form

$$\phi_R(r) = A \exp(-br) = \varepsilon\left(\frac{\sigma}{r}\right)^n \tag{2.6}$$

with A, b, ε and σ as parameters, gives the contribution E_R to the total energy:

$$E_R = \tfrac{1}{2} \sum_{\underline{R}_j \neq 0} \phi_R(\underline{R}_j) \tag{2.7}$$

Both the forms given above have been used to explain experimental results (Gibson et al. 1960, Lennard-Jones 1924). To correlate these two forms and for some of the transition metals, we have examined the radiation damage data and the melting curves of these metals.

Thus assuming the inverse power form for E_R, the total energy, in the simple metals takes the form

$$E_{sm} = E_C + E_V$$

$$= \sum_{ij} \phi_{eff}(r_{ij}) + E_V(V) \qquad (2.8)$$

with

$$\phi_{eff}(r) = \frac{A}{r^n} + \frac{B}{r^3} \cos(2k_F r + \theta) \qquad (2.9)$$

For the f.c.c. metals we have assumed the energy to be given by equation (2.8) with the interionic potential having the same form as in equation (2.9). We have, however, treated the constants in the potential as parameters.

Since we have assumed the ions to be spherically symmetric, upon melting, the metals acts like a classical liquid. Also since we do not expect the electronic distribution to change a great deal, the particles of the liquid would interact with each other through a potential that would be very nearly equal to ϕ_{eff}. However, the disorder present in the liquid would result in a damping of pair potential by a factor $\exp(-\lambda r)$, where λ is the inverse mean free path.

Now, in the theory of classical liquids, the X-ray (neutron) structure factor is related to the radial distribution function through the equation

$$S(\underline{k}) = 1 + \rho \int [g(r) - 1] \exp(i\, \underline{k}.\underline{r})\, d\underline{r} \qquad (2.10)$$

Various theories of classical liquids relate the direct correlation function, C(r), defined by the equation

$$C(r) = g(r)\,(1 - \exp(\phi(r)/k_B T)) \qquad (2.11)$$

to the effective pair potential, $\phi(r)$, asymptotically

$$C(r) \sim -\phi(r)/k_B T \qquad (2.12)$$

By the method of molecular dynamics (Verlet 1967) the pair potential obtained from the liquid structure factor may be refined so that it reproduces the input data. Thus,

we are able to determine an approximate $\phi(r)$ from the experimentally observed S(k).

In the next section we derive expressions for the elastic constants and phonon frequencies in cubic metals in which the total energy is given by equation (2.8). The short range repulsive potential is examined in §2.3 and values for the repulsivity, n, are estimated for the transition metals. Ni and Pt are examined in some detail in §2.4 and §2.5 and central pair potentials which reproduce experimental data are constructed. Finally in §2.6 we discuss the validity of central pair forces in the f.c.c. metals and the necessity of the inclusion of $E_V(V)$ in the expression for the total energy.

§2.2 Expressions for Elastic Constants and Phonon Dispersion Curves

We first derive expressions for the elastic constants of a cubic crystal, assuming that the energy is given by equation (2.8), by the method of homogeneous deformation of Fuchs (1936). We then derive an expression for the dynamical matrix and hence, the equations governing the phonon dispersion curves.

a) The elastic constants of a cubic crystal

From equation (2.8) the energy per unit undeformed volume of a monatomic crystal can be written as

$$U = \frac{1}{2\Omega_o} \sum_s \phi(R^s) + \varepsilon_V(V) \qquad (2.13)$$

where (R^s) is the value of the central pair potential in equation (2.9) at the s^{th} neighbour shell. Ω_o is the undeformed atomic volume and

$$\varepsilon_V(V) = \frac{E_V(V)}{N\Omega_o} \qquad (2.14)$$

N being the total number of atoms.

The elastic constants of a crystal are defined as the

coefficients in the expansion in powers of the Lagrangian strain, η_{ij}, of the change in the internal energy density, due to a homogeneous deformation.

Then writing the change in the internal energy density in the form

$$\Delta U = \eta_{ij} C_{ij} + \tfrac{1}{2} \eta_{ij}\eta_{kl} C_{ijkl} + \frac{1}{6} \eta_{ij}\eta_{kl}\eta_{mn} C_{ijklmn} + \cdots\cdots \tag{2.15}$$

the coefficients C_{ij}, C_{ijkl} and C_{ijklmn} are the first, second and third order elastic constants respectively, and are evaluated at zero strain.

But, in the approximation of equation (2.8), the change in internal energy can be written as

$$\begin{aligned}\Delta U = & \left(B_{ij} + \varepsilon' \delta_{ij}\right) \eta_{ij} \\ & + \tfrac{1}{2} \left(B_{ijkl} + \left(\varepsilon_v' + \varepsilon_v''\right)\delta_{ij}\delta_{kl} - 2\varepsilon_v' \delta_{jk}\delta_{il}\right) \eta_{ij}\eta_{kl} \\ & + \frac{1}{6} \left(B_{ijklmn} + \left(\varepsilon_v' + 3\varepsilon_v'' + \varepsilon_v'''\right)\delta_{ij}\delta_{kl}\delta_{mn}\right. \\ & - 6 \left(\varepsilon_v' + \varepsilon_v''\right)\delta_{il}\delta_{jk}\delta_{mn} \\ & \left. + 8\, \varepsilon_v' \, \delta_{in}\delta_{jk}\delta_{lm}\right) \eta_{ij}\eta_{kl}\eta_{mn}\end{aligned} \tag{2.16}$$

where

$$\left.\begin{aligned} B_{ij} &= \frac{1}{2\Omega_o} \sum_s \frac{1}{r} \frac{d\phi}{dr}\bigg|_o R_i^s R_j^s \\ B_{ijkl} &= \frac{1}{2\Omega_o} \sum_s \frac{1}{r} \frac{d}{dr}\left(\frac{1}{r}\frac{d\phi}{dr}\right)\bigg|_o R_i^s R_j^s R_k^s R_l^s \\ B_{ijklmn} &= \frac{1}{2\Omega_o} \sum \frac{1}{r} \frac{d}{dr}\left(\frac{1}{r}\frac{d}{dr}\left(\frac{1}{r}\frac{d\phi}{dr}\right)\right)\bigg|_o R_i^s R_j^s R_k^s R_l^s R_m^s R_n^s \end{aligned}\right\} \tag{2.17}$$

and

$$\varepsilon_v^{(n)} = V^n \frac{d^n \varepsilon_v}{dV^n} \tag{2.18}$$

Comparing equations (2.15) and (2.16) and taking account of the symmetry conditions, we find that the second order elastic constants are given by the equations:

$$C_{11} = \frac{1}{2\Omega_o} \sum_s \psi''(r^s)(x^s)^4 + \varepsilon_v'' - \varepsilon_v' \tag{2.19}$$

$$C_{12} = \frac{1}{2\Omega_o} \sum_s \psi''(r^s)(x^s)^2(y^s)^2 + \varepsilon_v'' + \varepsilon_v' \tag{2.20}$$

$$C_{44} = \frac{1}{2\Omega_o} \sum_s \psi''(r^s)(x^s)^2(y^s)^2 - \varepsilon_v' \tag{2.21}$$

with the equilibrium condition

$$C_1 = \frac{1}{2\Omega_o} \sum_s \psi'(r^s)(x^s)^2 + \varepsilon_v' \tag{2.22}$$

where

$$\psi^{(n)}(r^s) = \left[\frac{1}{r^s}\frac{d}{dr^s}\right]^n \phi(r^s)$$

The Cauchy discrepancy Martin (1975) is then

$$C_{12} - C_{44} = \varepsilon_v'' + 2\varepsilon_v' \tag{2.23}$$

We note that for $\varepsilon_v = 0$, i.e., for central forces, this discrepancy is zero, which is just what we would expect.

The equations for the third order elastic constants follow naturally

$$\left.\begin{aligned}
C_{111} &= \frac{1}{2\Omega_o} \sum_s \psi'''(r^s)\cdot(x^s)^6 + 3\varepsilon_v' - 3\varepsilon_v'' + \varepsilon_v''' \\
C_{112} &= \frac{1}{2\Omega_o} \sum_s \psi'''(r^s)\cdot(x^s)^4(y^s)^2 - \varepsilon_v' + \varepsilon_v'' + \varepsilon_v''' \\
C_{166} &= \frac{1}{2\Omega_o} \sum_s \psi'''(r^s)\cdot(x^s)^4(y^s)^2 + \varepsilon_v' - \varepsilon_v'' \\
C_{144} &= \frac{1}{2\Omega_o} \sum_s \psi'''(r^s)\cdot(x^s)^2(y^s)^2(z^s)^2 - \varepsilon_v' - 3\varepsilon_v'' \\
C_{123} &= \frac{1}{2\Omega_o} \sum_s \psi'''(r^s)\cdot(x^s)^2(y^s)^2(z^s)^2 + \varepsilon_v' + 3\varepsilon_v'' + \varepsilon_v''' \\
C_{456} &= \frac{1}{2\Omega_o} \sum_s \psi'''(r^s)\cdot(x^s)^2(y^s)^2(z^s)^2 + \varepsilon_v'
\end{aligned}\right\} \tag{2.24}$$

A little algebraic manipulation leads to

$$C_{12} - C_{44} = C_{456} - C_{144} = C_{166} - C_{112} + C_{123} - C_{456}$$

$$= 2\varepsilon_v' + \varepsilon_v'' \qquad (2.25)$$

which is a generalised Cauchy condition for the model described by equation (2.8). This condition provides a measure of the suitability of the approximation made in equation (2.8) for particular cubic metals.

b) Phonon Frequencies

In the harmonic, and pair potential approximation the phonon frequencies, $\omega(\underline{k})$ are given by the equation

$$\omega^2(k)\, U_\alpha(\kappa) = \sum_{\kappa'\beta} D_{\alpha\beta}\,(\kappa\kappa'|\underline{k})\, U_\beta(\kappa') \qquad (2.26)$$

where the dynamical matrix $D(\underline{k})$ is defined by the relation

$$D_{\alpha\beta}(\kappa\kappa'|k) = \frac{\sum_{1'} W_{\alpha\beta}\begin{bmatrix}o1'\\ \kappa\kappa'\end{bmatrix} \exp\left(-i\underline{k}\cdot(\underline{x}(o) - \underline{x}(1'))\right)}{\left[M_\kappa M_{\kappa'}\right]^{\frac{1}{2}}} \qquad (2.27)$$

with

$$W_{\alpha\beta}\begin{bmatrix}o1'\\ \kappa\kappa'\end{bmatrix} = \frac{\partial^2 W}{\partial U_\alpha\begin{bmatrix}o\\ \kappa\end{bmatrix} U_\beta\begin{bmatrix}1'\\ \kappa'\end{bmatrix}} \qquad (2.28)$$

W is the potential energy of the crystal and $U_\alpha\begin{bmatrix}l\\ \kappa\end{bmatrix}$ is the displacement is the α direction of the κ^{th} basis atom, of mass M_κ, in the 1^{th} unit cell.

From equations (2.27) and (2.29) it follows that

$$D_{\alpha\beta}(\kappa\kappa'|\underline{k}) = \sum_{1'} \frac{\delta_{o1'}\delta_{\kappa\kappa'}}{(M_\kappa M_{\kappa'})^{\frac{1}{2}}} \sum_{st} \phi_{\alpha\beta}\begin{bmatrix}os\\ kt\end{bmatrix}\left[1 - \delta_{so}\,\delta_{tk}\right]$$

$$- \left(1 - \delta_{o1'}\,\delta_{\kappa\kappa'}\right) \phi_{\alpha\beta}\begin{bmatrix}o\ 1'\\ \kappa\ \kappa'\end{bmatrix} \times$$

$$\times \exp\left(-\,i\,\underline{k}\cdot(x(o) - x\,(1'))\right) +$$

$$+ \sum_{1'}^{*} \frac{3V}{r^2\begin{bmatrix}1'\\k'\end{bmatrix}} \left[\frac{r_\alpha\begin{bmatrix}1'\\k'\end{bmatrix} r_\beta\begin{bmatrix}1'\\k'\end{bmatrix}}{r^2\begin{bmatrix}1'\\k'\end{bmatrix}} (3\varepsilon_v'' + 7\varepsilon_v' + \varepsilon_v) + \delta_{\alpha\beta}(\varepsilon_v' + \varepsilon_v) \right]$$

where the asterisk denotes the sum is only taken over $\begin{bmatrix}1'\\k'\end{bmatrix}$ and $\begin{bmatrix}o\\\kappa\end{bmatrix}$ being nearest neighbours.

§2.3 The short range potential

We showed in the introduction to this chapter that the short range repulsive potential between two ions when they are brought close together can be written as

$$\phi_R(r) = \frac{B}{r^n} \equiv A \exp(-br) \qquad (2.30)$$

By studying various experimental data, we estimate the value of n for some f.c.c. transition metals.

a) Radiation Damage

Various workers have studied the displacement threshold energies in radiation damage and the work has been extensively reviewed by Vajda (1977). The measured threshold energies of a number of metals have been found to be consistent with the parameter b in equation (2.6), taking values between 4 and 6 A^{o-1}. Anderson and Sigmund (1965) approximately represented the short range interaction between two atoms in the metal by the form

$$\phi_R(r) = A_o Z^{3/2} \exp(-br) \qquad (2.31)$$

where Z is the atomic number and A_o and b have values 52eV and 4.56 A^{o-1} respectively.

b) The melting temperature at zero external pressure

The simplest and most successful theory of melting is that of Lindemann (1910). In this theory, the solid-liquid transition occurs when the root mean square displacement of

each lattice atom due to thermal agitation, becomes about a tenth of the nearest neighbour distance.

All theories of melting which take into account the potential between atoms show that the melting temperature T_{melt}, is proportional to the strength of the potential (Hoover and Ross, 1971). Thus, for the inverse power potential given in equation (2.30)

$$T_{melt} = \alpha \frac{\epsilon}{k_B} \tag{2.32}$$

where α is some constant.

In order to relate this to the Born-Mayer potential we first equate the two forms of the potential in equation (2.30) in the energy range over which they are valid, we find that for the f.c.c. metals.

$$n = \frac{(\sqrt{3}-1)}{\ell n 3} ab \tag{2.33}$$

and

$$\epsilon = A \left(\frac{a}{2\sigma}\right) \exp(-ab/2) \tag{2.34}$$

Thus, the melting temperature is related to the Born-Mayer parameter, b, by the equation

$$\frac{T_{melt}}{Z^{3/2}} = \frac{\gamma_f \exp(-ab/2)}{(0.9\sqrt{2})^{(\sqrt{3}-1)\, ab/\ell n 3}} \tag{2.35}$$

where γ_f is some constant.

In figure 2.1 we have plotted $T_{melt}/Z^{3/2}$ against ab from equation (2.35) for some f.c.c. transition metals, with b taken to be 4.56 A^{o-1}. The small deviation of the experimental points from the curve indicates the usefulness of the forms of the potential given in equation (2.30)

Fuchs (1936) and Huntington (1953), who used the Born-Mayer form of the potential to calculate the elastic constants of Cu, estimated the parameter b to be between 6 and 7. This results in n taking values between 14 and 17. Radiation

Figure 2.1

Melting temperatures at atmospheric pressure correlated with parameters A_o and b in the equation form of the repulsive interactions, a is the cubic spacing and Z is the atomic number.

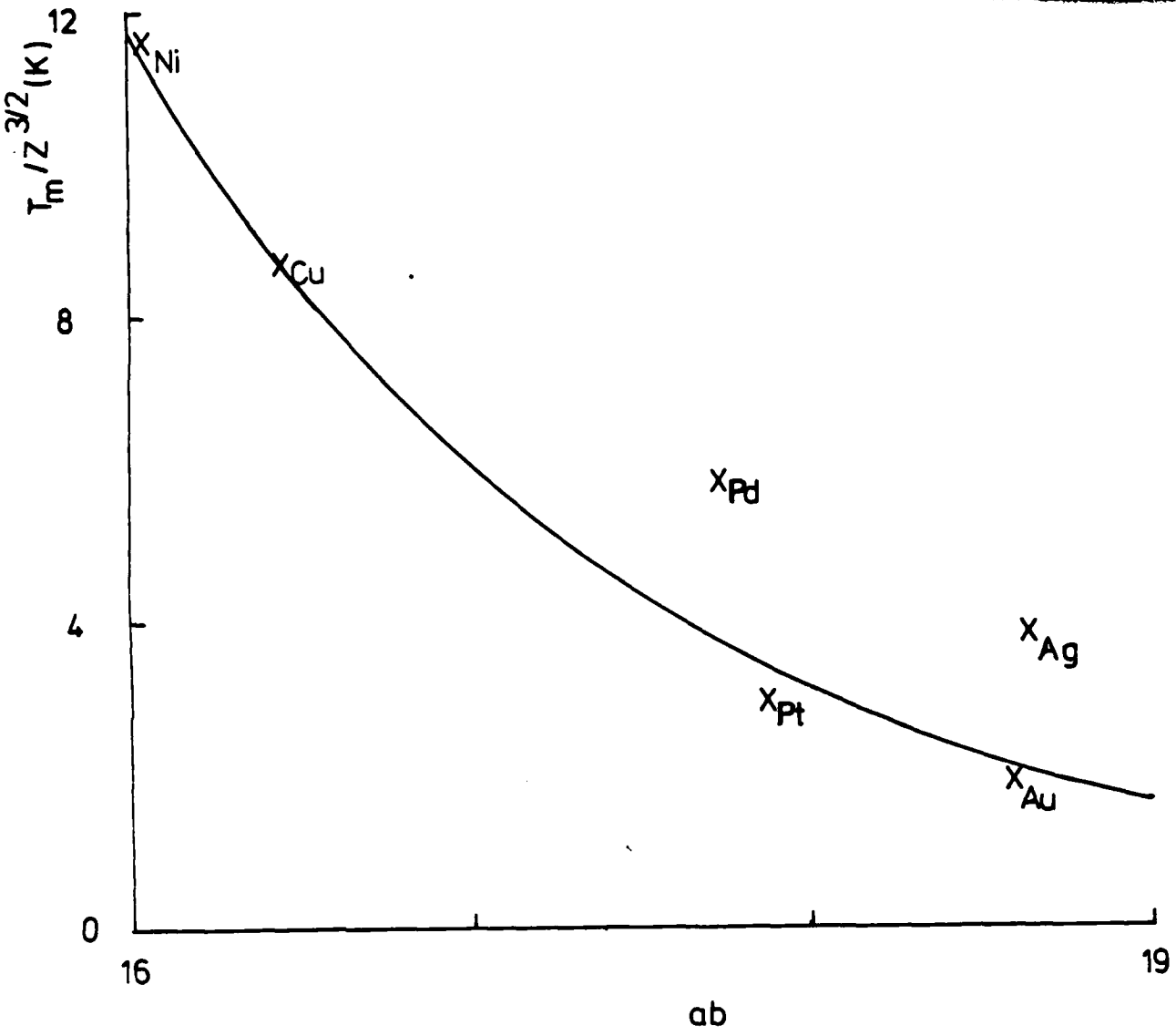

damage analysis of the transition metals (Vajda 1977) also leads to values of b consistent with the above. The hardness of the core of the transition metal can also be found if we examine the data of melting temperatures at high pressures.

c) Melting curves under pressure

It can be shown (Hoover and Ross 1971) that for purely repulsive potentials of the form $1/r^n$ the melting curve is consistent with a Simon coefficient (Simon 1937), c, given by

$$c = 1 + 3/n \qquad (2.36)$$

The melting data of the transition metals (see for example Cannon 1974) shows that c is only very slightly larger than unity, implying a large value of n.

Thus all the experimental evidence shows that n, for the transition metals is of the order of 16.

§2.4 Pair potentials and Phonon Frequencies in Ni

Johnson et al. (1976) obtained a pair potential for liquid Ni from the measured neutron scattering structure factor data. The potential, they reported, was modified slightly so that it reproduced the experimentally determined radial distribution function in a molecular dynamics calculation. We have used this as a starting point in our attempt to calculate a central pair potential for Ni.

It is, of course, recognised that in Ni the force fields may well be different in the liquid and solid states since:

a) There is a volume change on melting and one expects from the basic theory that interionic potentials will be density dependent. This is a direct consequence of the definition of the pair potential.

b) The Fermi surface, enclosing the electrons which screen the Ni ions in the metal, has a complicated shape in the crystal. One would expect, in contrast, the Fermi surface in the liquid to be isotropic. Naturally, on melting

detailed changes will, therefore, occur in the screening and hence, in the effective interionic potential.

c) The electronic mean free path is shorter in the liquid than in the solid. Oscillations, due to the incomplete screening of ions, will therefore, from the Uncertainty Principle, be more heavily damped in the liquid than in the solid.

In view of our present lack of knowledge of the interionic forces in the transition metals, we have assumed that the changes due to (a) and (b) above, are hardly likely to be larger than the uncertainties in such potentials. The effect of the greater mean free path in the liquid can be accounted for by multiplying the effective interionic potential by an exponential damping factor.

We have studied, therefore, how well

(i) the elastic constants

(ii) the phonons throughout the BZ

can be reproduced, by making small changes in the potential extracted from the liquid.

From the arguments given in §2.1 we expect the central pair potential in Ni to have the form given by equation (2.9)

$$\phi(r) = \frac{A}{r^n} + \frac{B}{r^3} \cos (2k_F r + \theta)$$

To take account of the electronic mean free path this equation can be modified to read

$$\phi(r) = \frac{A}{r^n} + \frac{B}{r^3} \cos (2k_F r + \theta) \exp (-\lambda r) \qquad (2.37)$$

where λ is the inverse of mean free path

From §2.3 we argued that n was of the order of 16. To obtain the other parameters in the potential we have relied on the liquid pair potential of Johnson et al. (1976). The values of k_F and θ were estimated from the wavelength and nodal positions of the long range part of the liquid potential. Neglecting λ, A and B were determined by fitting

the position and depth of the first minimum of this potential. These values are tabulated in table 2.1.

The mean free path, L, in liquids is about twice the nearest neighbour distance. In solids the mean free path is much greater, and we have assumed the ratio of the mean free path in the liquid to that in the solid, to be of the order of the ratio of the room temperature to the melting temperature. Hence, $L_{solid} \sim 5\ L_{liquid}$. This gives λ a value of about $0.05 A^{o-1}$ in solid Ni.

The contribution of this potential to the phonon frequencies was calculated by the use of equations (2.26) to (2.29). The potential was truncated at the fourth neighbour distance and λ was taken to be zero. We have in fact calculated $\omega(\underline{k})$ at different cut-offs (up to $35.2 A^{o}$) with a finite value of λ and the discrepancies between the results were found to be less than 5%, well within the range of experimental uncertainties. However, we find that with this potential, $\lambda(k)$ in some modes turn out to be imaginary, indicating some kind of instability in the solid when phonons are propagated along these directions. To remove these instabilities, we have varied A, B and θ with the constraint that the depth of the first minimum is kept roughly the same. The new values of the parameters are also tabulated in table 2.1 under the column entitled 'solid'. The depth of the first minimum was kept the same because it is related to the height of the first peak in the g(r) of the liquid, which we require to be the same. Both these potentials are drawn in figure 2.2. It is interesting to note that the 'solid potential' has its minimum displaced slightly. A simple way in which the potential can be made density dependent is by scaling the interatomic distances. The volume change on melting would, thus, result in the distance of the first minimum in the liquid potential being fractionally greater than that of the 'solid potential', which is consistent with our potentials for Ni.

TABLE 2.1

Parameters of the solid and liquid potentials in Ni.

PARAMETER	LIQUID	SOLID
A (eV $\mathring{A}^{16}$)	44351.0	40319.0
B (eV $\mathring{A}^{3}$)	2.26	2.06
$2k_f$ ($\mathring{A}^{-1}$)	3.25	3.25
θ	0.994	1.600

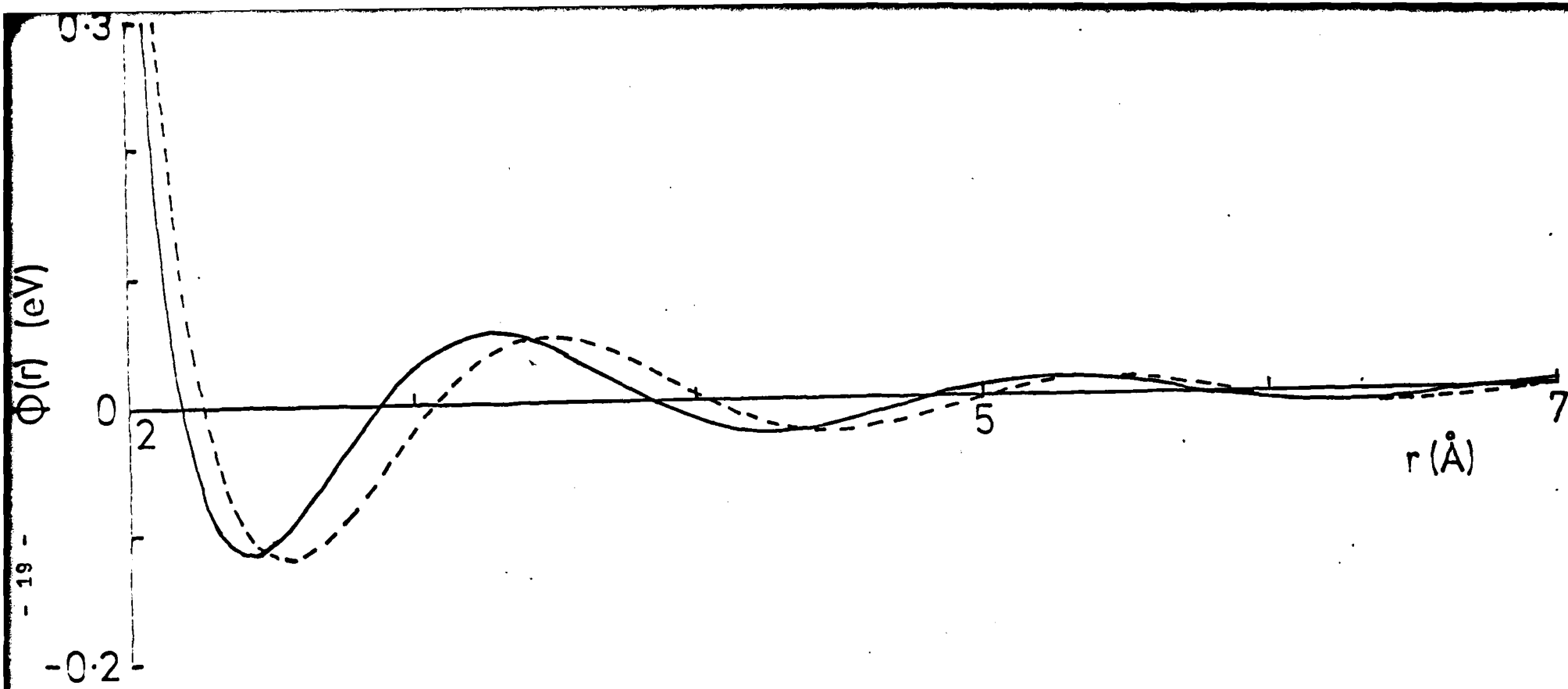

Figure 2.2

Pair potentials for liquid (dashed) and solid (full curve) Ni.

Having obtained a reasonable central pair potential, phonon dispersion curves were recalculated with the inclusion of the volume dependent energy. $E_v(V)$ was represented by the semi-empirical form

$$E_v(V) = \frac{d}{V^{2/3}} \tag{2.38}$$

which was prompted by the free electron volume dependence. Of course, this does not have a first-principle justification for the transition metals, but it appears adequate for our present purposes. The parameter d was determined from the equilibrium condition expressed by equation (2.22).

We have plotted in figure 2.3 for Ni the calculated $\omega(k)$, with and without the inclusion of E_v, versus k in the three symmetry directions together with the experimental points (Birgeneau et al. 1964). The dashed lines are those curves calculated from the central pair potential of the solid and the full lines are those obtained with the inclusion of E_v. It may be observed that the term, E_v, provides a necessary contribution to $\omega(k)$, to bring it in agreement with the experimental data.

From the nature of E(V) discussed in §2.1, we see that d in equation (2.38) must be positive. The actual form may not be unique, but the representation of $E_v(V)$ by a single volume dependent term is the most useful, as the one parameter is fixed by the equilibrium condition. We have repeated the calculations for different forms of E_v, namely,

$$E_v(V) = d/V^m \tag{2.39}$$

where m was of the order of unity.

The changes in the phonon frequencies from the m = 2/3 case proved to be quite insignificant.

We have also calculated the second order elastic constants of Ni with and without the inclusion of $E_v(V)$, and these are shown in table 2.2, together with the experi-

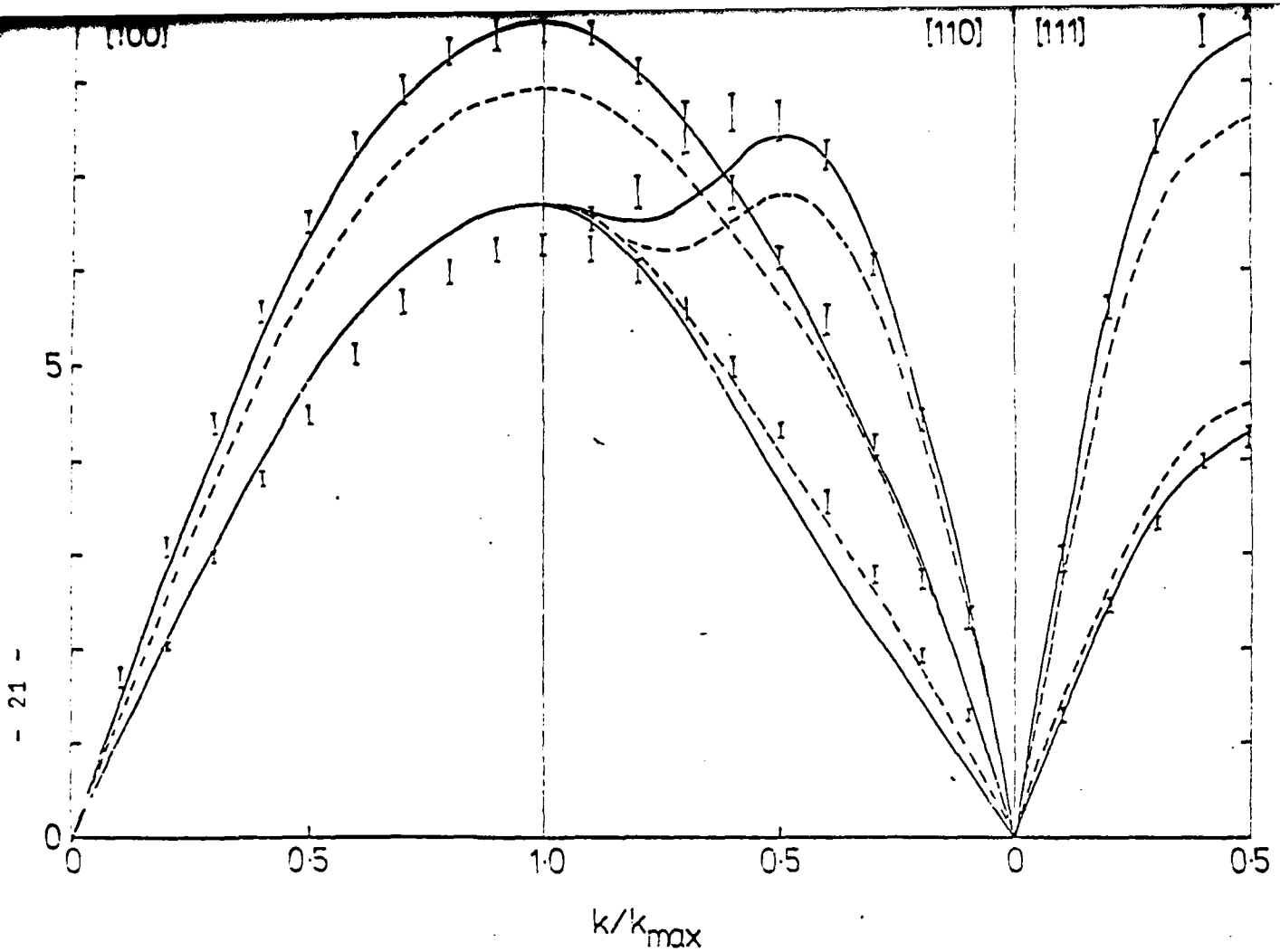

Figure 2.3

Phonon dispersion curves for f.c.c. Ni, with potential shown in solid curve of Figure 2.2, plus volume dependent energy. The dashed curves show the effect of omitting volume-dependent energy. For the (100) transverse modes, the volume-dependent energy does not alter the dispersion curve.

TABLE 2.2

Second order elastic constants and
bulk modulus B for f.c.c. Ni.

$C_{ij}(10^{10}N/m^2)$	E(V) = 0	$E(V) = \frac{d}{V^{2/3}}$	Expt. (a)
C_{11}	18.9	24.1	24.6
C_{12}	11.7	14.1	15.0
C_{44}	11.7	13.2	12.2
B	14.1	17.4	18.6

(a) de Klerk (1959).

mental values (de Klerk 1958). The positive d in equation (2.38) gives a positive Cauchy discrepancy in accordance with experiment.

The radial distribution function for Ni using the 'solid potential' was generated by a molecular dynamics calculation. The resulting g(r) does not differ significantly from that obtained from the liquid potential.

§2.5 Pair Potentials, Phonon Frequencies and Liquid Structure Factor in Pt

Recent neutron inelastic scattering measurements from H adsorbed on a Pt surface by Wright et al. (1976) have been interpreted in general terms by Mahanty et al. (1976). It is clear from their work that a quantitative interpretation of the neutron results will require knowledge of the long range interionic potential for Pt. We have, therefore, attempted to construct an interionic potential for Pt.

The arguments presented in §2.3 which led us to choose the repulsivity of Ni to be 16, also apply to Pt. This is especially true of the data on the melting curves under pressure. With this value of n, the parameters A and B were adjusted, so that the first minimum of the potential appeared at about the nearest neighbour position in Pt with depth approximately equal to that in Ni. An initial value for $2k_F$ was estimated from the value for Ni, but with the increased atomic volume taken into account. The phonon frequencies in the three symmetry directions were calculated with this potential. The values of $2k_F$ and θ were then varied until a good fit to the phonon dispersion curves was obtained. We were, thus, able to find a useful representation of the central pair potential in Pt, namely.

$$\phi(r) = \frac{409732}{r^{16}} + \frac{3.29}{r^3} \cos(3.49r + 1.55) \qquad (2.40)$$

where r is measured in A^o, and the potential is truncated at the fourth neighbour distance. This potential is

plotted in figure 2.4.

Then, including $E_v(V)$ in the form given by equation (2.38), the phonon frequencies were recalculated and the results are shown in figure 2.5, together with the experimentally measured values (Dutton et al. 1972). Unlike in the case of Ni, the effect of E_v turns out to be quite small.

The general agreement between the calculated and experimental values, with the exception of the pronounced Kohn anomaly in the (110) direction, is very good. It may be that to reproduce the Kohn anomaly, one would need to take account of the long range oscillatory tail. However, if this were the case, Kohn anomalies would also appear in the theoretical calculations of the dispersion curves of Ni. That this is not experimentally observed leads one to think that it is the detail of the Fermi surface that is important (see for example Flores et al. 1979).

Recently, Tripathi and Nand (1979) calculated the phonon frequencies of Pt using a model potential approach. Though their results are in fair agreement with experiment, they were unable to reproduce the Kohn anomaly. This is in spite of the fact that their calculations were made in reciprocal space and so took account of the long range tail. Their estimates of the magnitude of the anomaly turns out to be very small. Their calculations, thus, show that the inclusion of the long-range tail does not necessarily result in observable Kohn anomalies and the observation of such should be attributed to the details of the Fermi surface.

We have also calculated the second order elastic constants of Pt and these are tabulated together with the experimental values (Gschneider 1964) in table 2.3. Again, we note that E_v does not appear to make any significant contribution. The truncation of the interatomic potential is not a good approximation in the evaluation of the elastic constants, because from equations (2.19) to (2.21) we see that the expressions for them are not absolutely convergent if the mean free path, $1/\lambda$, is infinite.

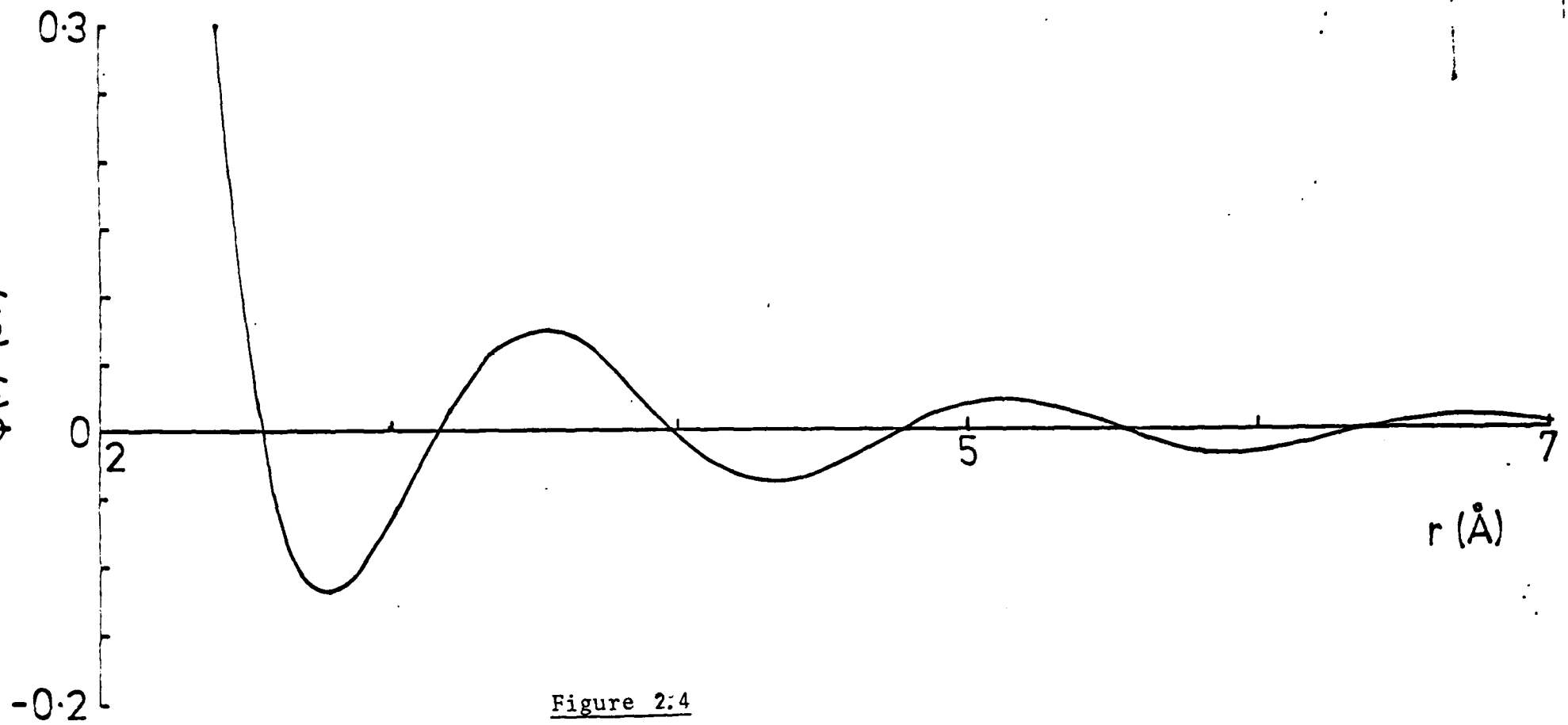

Figure 2.4

Pair potential for solid Pt.

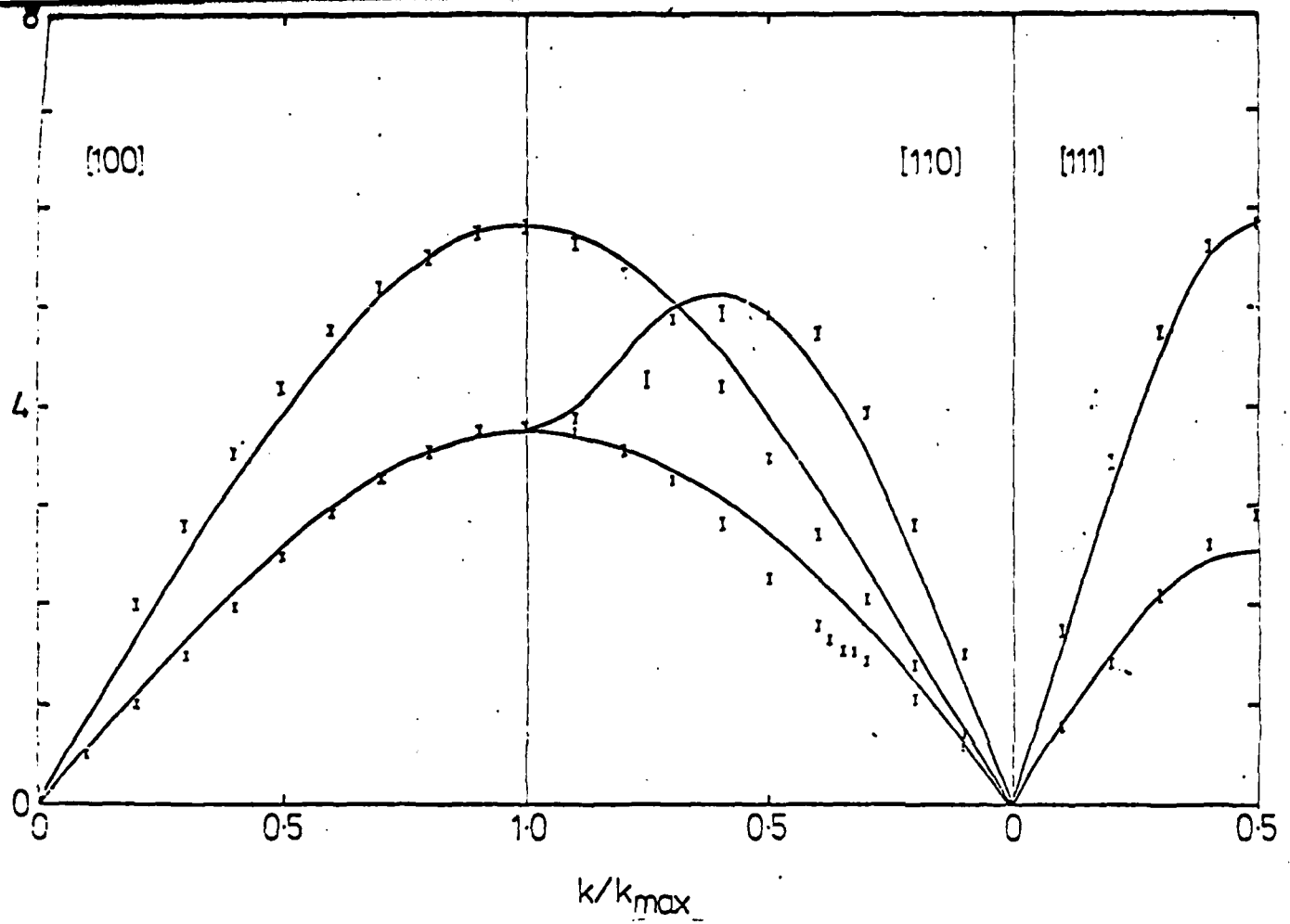

Figure 2.5

Phonon dispersion curves for f.c.c. Pt. The influence of the volume-dependent energy, included in the curves shown, is in fact small. Experimental results from Dutton et al. (1972).

TABLE 2.3

Second order elastic constants and
bulk modulus B for f.c.c. Pt.

$C_{ij}(10^{10}N/m^2)$	E(V) = 0	$E(V) = \frac{d}{V^{2/3}}$	Expt. (a)
C_{11}	22.8	23.4	
C_{12}	9.9	10.2	
C_{44}	9.9	10.0	
B	14.2	15.6	27.8

(a) Gschneider (1964).

In contrast with our work on Ni, we decided to test our potential in Pt, obtained by fitting the phonon frequencies, by calculating the liquid S(k) and comparing it with experiment.

From equation (2.40) we see that the core is very hard, so we expect S(k) to have the main features of the known hard sphere form. This latter result is independent of temperature, depending only on the ratio of the volume occupied by the hard spheres to the total volume (Ashcroft and Lekner 1966). We, therefore, ran a moleculer dynamics program at a higher temperature than the known melting temperature of Pt, to ensure that the solid had melted.

In the program, the system consisted of 256 particles interacting between themselves through the central pair potential given by equation (2.40). The system was allowed to evolve for five hundred time steps, each of 10^{-15} seconds. The time interval was chosen such that the total energy of the system was conserved to four significant figures. The mean temperature was then calculated over the next two hundred time step intervals to verify that equilibrium had indeed been reached. At the end of each time interval the g(r) and its fourier transform, S(k) were calculated according to equation (2.10). There was no significant difference at each time interval.

We have plotted S(k) versus k for Pt in figure 2.6. The crosses indicate the positions of the maxima and minima of the experimental results of Waseda and Ohtani (1975a).

The close agreement between the results indicates that the potential given by equation (2.40) also provides a good description of the liquid state.

Another interesting observation is that the agreement is very good even at the third peak. The long range part of S(k) is dependent on the repulsivity, therefore, this agreement is a vindication of our choice of n for Pt.

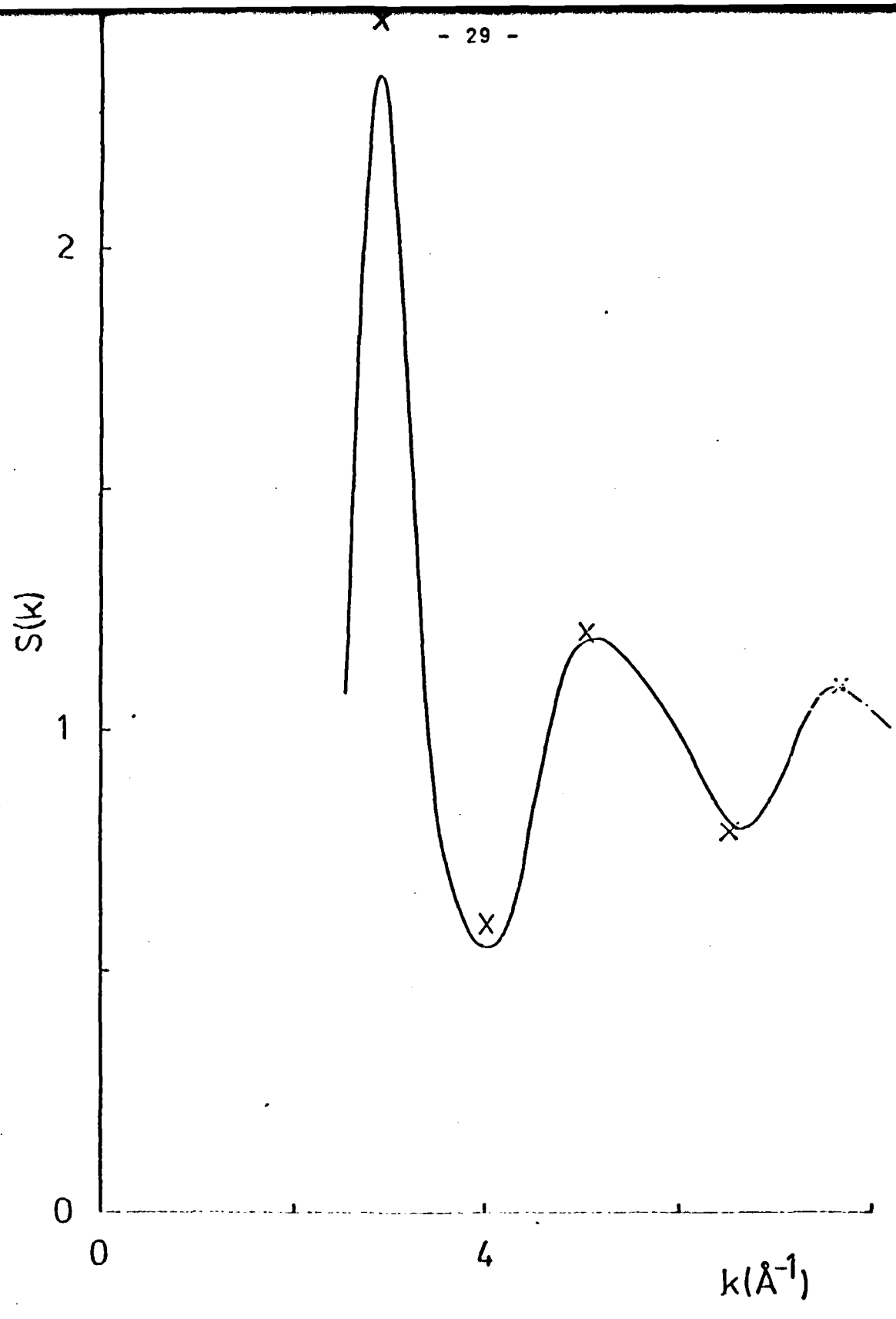

Figure 2.6

Liquid structure factor for Pt. The structure factor is similar to a hard sphere form. The experimental results are from Waseda and Ohtani (1975a).

§2.6 Discussion

In the above sections we have obtained central pair potentials for Ni and Pt. The usefulness of these pair potentials depends on the validity of the approximation expressed by equation (2.8). We have also assumed that the central pair forces in the solid and liquid states are very nearly the same. We now consider whether these approximations are good in the f.c.c. transition metals.

In §2.2 we saw that if the approximation represented by equation (2.8) is to be valid, in any cubic metal, then their second and third order elastic constants must satisfy equation (2.25). Since this work was first completed (Matthai 1978a) Cousins and Martin (1978) showed, by considering inner displacements in a crystal, that the linear combination of elastic constants

$$Q_3 = C_{12} - C_{44} + C_{144} - C_{456} \qquad (2.41)$$

and

$$Q_6 = 2(C_{12} - C_{44}) - C_{123} + C_{144} + C_{112} - C_{166} \qquad (2.42)$$

are devoid of contributions from central or isotropic interactions. This is completely consistent with our equation (2.25)

We have tabulated in table 2.4, the three linear combinations of elastic constants appearing in equation (2.25) as determined from experiment for some f.c.c. metals for which the third order elastic constants have been measured and for directionally bonded diamond-type Si and Ge. Although these conditions are not satisfied by any of the solids considered, it appears that it is a better approximation in the f.c.c. metals than in Si or Ge. It should be noted that the errors in the measurements of the third order elastic constants are quite large.

TABLE 2.4

Combinations of elastic constants for f.c.c. metals and semiconductors Si and Ge (in $10^{11} N/m^2$).

	$C_{12}-C_{44}$	$C_{456}-C_{144}$	$C_{166}-C_{112}+C_{123}-C_{456}$
Cu[a]	0.44	-0.92	0.79
Ag[a]	0.45	0.27	-0.02
Au[a]	1.22	0.01	0.53
Ni[b]	0.29	1.38	6.89
Al[c]	0.32	-0.07	0.41
Si[d]	-0.16	-0.76	1.4
Ge[e]	-0.19	-.05	0.8

(a) Hiki and Granato (1966)
(b) Sarma and Reddy (1973)
(c) Thomas (1968)
(d) McSkimmin and Andreatch (1964)
(e) Drabble and Fendly (1967)

We have also calculated the third order elastic constants of Ni and they are tabulated with the experimental values in table 2.5. With the exception of C_{123}, the agreement between the two sets of values is very good, especially if one recognises that to obtain the third order elastic constants one requires the third derivative of the inter atomic potential.

This gives added weight to our assumptions that angularity in the force fields is less prevalent in the f.c.c. than in the b.c.c. transition metals. Thus, it would seem that with the phonon frequencies and liquid S(K) well reproduced, the idea of central pair forces in the f.c.c. transition metals is a useful one.

Another aspect of our work has been the explicit introduction to the volume dependent term in the total energy. This enabled us to determine its contribution to the elastic constants and the phonon frequencies. It also results in a positive Cauchy discrepancy for isotropic forces as is observed in most metals. Furthermore, by introducing the parameter d in equation (2.38), we were also able to satisfy the equilibrium condition given by equation (2.22) From our calculations, it turns out to be much smaller than the coefficient of the leading term in the free electron gas energy expansion. Previous workers were not able to satisfy the correct equilibrium condition and get reasonable phonon frequencies because of the form they used for E_v. A review of the literature shows that most workers have used incorrect equilibrium conditions with E_v as the free electron energy. Upadhyaya (1978) pointed this out, but suggested that to get a positive Cauchy discrepancy one needs to go to higher order in the perturbation. We have shown that this need not be the case if E_v were not just the free electron energy and that part arising from charge neutrality, but also consisted of other many body terms, which are averaged out to make an isotropic contribution.

TABLE 2.5

Third order elastic constants for Ni (10^{11}N/m^2)

	Calculated including E_v(V)	Expt. [a]
C_{111}	-10.62	-21.04
C_{112}	- 7.50	-13.45
C_{144}	- 1.22	- 1.80
C_{166}	- 7.28	- 7.57
C_{123}	- 1.32	+ 0.59
C_{456}	- 1.16	- 0.42

(a) Thomas (1968)

Finally, we conclude this chapter with some comments on the accuracy of the pair potentials obtained. Variations on the accuracy of the parameters A, B, k_f and θ result in changes in the dispersion curves. In so far as the phonons with $k \neq 0$ accurately determine a potential, we estimate these parameters to be accurate to better than 5%. However, this is for a fixed value of λ. Because of the truncation of our potential, a further uncertainty due to the parameter λ is also introduced. So, before claims of an accurate potential can be made, the actual value of λ is required.

CHAPTER 3

The angularity of the charge distribution (force fields) in metals

§3.1 Introduction

From linear response theory, it follows that the force fields in metals are directly related to the charge distribution. Although we assumed that central forces provide a good description of the f.c.c. transition metals, and showed that the assumption to be a good one in calculating the elastic constants, phonon frequencies and the liquid structure factor; we realise that a full description of the force fields would have to take account of the angularity in the charge distribution. This angularity is most easily discernible in the b.c.c. transition metals. The inadequacy of the central pair potential model for the b.c.c. transition metals is most apparent in the behaviour of their elastic constants and phonon dispersion curves.

With the assumption of a central pair potential plus a volume dependent energy, we saw that the calculated Cauchy discrepancy, $C_{12} - C_{44}$, will be small and positive. An examination of the second order elastic constants of the b.c.c. transition metals reveals that their Cauchy discrepancies, though positive (with the exception of Cr), differ a great deal in magnitude. Alone among the metals, Cr displays a negative discrepancy, a feature also found in the covalently bonded solids, Si and Ge. From our formulation of E_v, this can never arise as d given by equation (2.38) is taken to be positive and so to correct this deficiency in the model, angular forces must also be included in the expression for the total energy. It further indicates that perhaps this angularity can be represented in terms of bond hybrids.

Further evidence of the angularity in the b.c.c. transition metals, from an observation of certain linear combinations of elastic constants, has been given by Chikazumi

(1979). By appealing directly to the measured second order elastic constants, he was able to show that for Ni the atomic force is almost central, wheras he concluded that the atomic shape of the Fe atom in the low spin state is anisotropic.

Brockhouse et al. (1967) made a Born-von Karman force constant fit to the phonon dispersion data of Fe, and found that the 1XX component was greater than the 1XY component. They interpreted this as being indicative of an attractive force between nearest neighbours. This observation was confirmed by Minkiewicz et al. (1967). Brockhouse et al. also observed that the 1XX component was greater than the 1XY component for all the b.c.c. transition metals that had been investigated. Interestingly, they found the opposite inequality, which implies repulsive forces between nearest neighbours, as would be intuitively expected to be true in the non-transition b.c.c. metals. Analysis of all the f.c.c. metals also show first neighbour repulsion. These facts rather strongly suggest that in the b.c.c. transition metals, the d-electrons are involved in some kind of quasi-covalent bonding.

Considerable information about the charge density can be obtained from an analysis of the X-ray scattering factor data of solids. A useful way of extracting this information is to compare the X-ray scattering results from the solid state with the free atom prediction. This tells us how the basic building block in the solid suffers from that in the free atomic state.

In the rare gas solids (Ar, Kr and Xe) the measured scattering factors show no difference from the free atom results, which is in agreement with the theory that in the solid state the building blocks are still the free atoms. A derivation from the free atom results is, however, observed in the simple and d-band metals and the covalently bonded solids.

In covalently bonded Si, once angularity is put into the charge distribution around the ionic centre to take

account of the bonding, the discrepancy between the scattering factors in negligible (De Marco and Weiss 1965). This is in direct contrast with the metals, where the discrepancy persists even when angularity is introduced into the ionic centre charge distribution (Brown and Taylor 1969).

Batterman et al. (1960) measured the X-ray scattering factors of Fe, Cu and Al. Their results were found to be about 4% smaller than the calculated free atom scattering factors, with Fe showing the greatest discrepancy. Brown and Taylor (1969) suggested that this discrepancy is a feature of metallic bonding, which is responsible for the modification of the electronic charge distribution. Experiments by Paakari and Suortti (1967) on Fe, Hosoya and Yamagishi (1966) on Cu and Inkinen and Suortti (1964) on Ni confirmed the discrepancy between the measured and free atom values found by Batterman et al., although they found it to be much smaller. In Fe the discrepancy was found to be about 1.7% and extended up to values of $\sin\theta/\lambda = 0.5\text{Å}^{-1}$. The discrepancies in Cu and Ni are smaller and vanish almost completely at the second reflection, which is very close to the first one in angular position. This appears to indicate that the electronic redistribution in Fe is greater than in Cu or Ni.

In the next section we consider the theory of X-ray scattering from solids using a Wannier function formalism. In §3.3 we use the results obtained from this approach to interpret the experimental scattering data of the transition metals. We pay special attention to Fe because of the availability of reliable scattering data up to large scattering angles. We discuss the nature of the charge distribution in the transition metals and the implications on the force fields in §3.4

§3.2 X-ray Scattering in Solids in the Wannier Function Formalism

The X-ray scattering factor $S(\underline{k})$ is given by

$$S(\underline{k}) = \int_V \rho(\underline{r}) \exp(i\underline{k}.\underline{r})\, dr \qquad (3.1)$$

where $\rho(\underline{r})$ is the charge density of the crystal of volume V.

Let us consider a crystal of N atoms with ion core electronic wavefunctions, $\psi_c(r)$ and valence electrons, $\psi_k(r)$. The total charge density of the crystal is

$$\rho(\underline{r}) = \sum_n \sum_c \psi_c^*(\underline{r}-\underline{R}_n)\, \psi_c(\underline{r}-\underline{R}_n) + \sum_{\substack{\text{occupied} \\ \text{levels}}} \psi_{\underline{k}}^*(\underline{r})\, \psi_{\underline{k}}(\underline{r}) \qquad (3.2)$$

which we can write as

$$\rho(\underline{r}) = \sum_n \sigma(\underline{r}-\underline{R}_n) + \sum_{\substack{\text{occupied} \\ \text{levels}}} \psi_{\underline{k}}^*(\underline{r})\, \psi_{\underline{k}}^*(\underline{r}) \qquad (3.3)$$

where $\underline{R}_n$ is a lattice vector.

The $\psi_{\underline{k}}(\underline{r})$ are the Bloch functions (BF's) generated by the one-body periodic potential $V(\underline{r})$. This potential can be written in the form

$$V(\underline{r}) = V_h(\underline{r}) + \frac{\delta \varepsilon_{xc}[\rho]}{\delta \rho} \qquad (3.4)$$

where $V_h(\underline{r})$ is the Hartree potential and ε_{xc} the exchange and correlation energy which is a functional of the density.

For simplicity, we assume the valence band to be described by one occupied non-degenerate band. The BF's can then be written in terms of Wannier functions (WF's), $a(\underline{r}-\underline{R}_n)$, namely

$$\psi_k(\underline{r}) = N^{-1/2} \sum_n a(\underline{r}-\underline{R}_n) \exp(i\underline{k}.\underline{R}_n) \qquad (3.5)$$

the inverse transformation yields

$$a(\underline{r}-\underline{R}_n) = N^{-1/2} \sum_k \psi_{\underline{k}}(\underline{r}) \exp(-i\underline{k}.\underline{R}_n) \qquad (3.6)$$

Substituting equation (3.5) into the expression for the charge density, we find

$$\rho(\underline{r}) = \sum_{\underline{k}<\underline{k}_F} \rho_{\underline{k}}(\underline{r}) + \sum_n \sigma(\underline{r}-\underline{R}_n) \qquad (3.7)$$

where

$$\rho_{\underline{k}}(\underline{r}) = N^{-1} \sum_{nm} \exp(i\underline{k}.(\underline{R}_m-\underline{R}_n))\ a(\underline{r}-\underline{R}_m)\ a(\underline{r}-\underline{R}_n)$$

and $\underline{k}_F$ is the Fermi wavevector which defines the boundary of the Fermi surface.

To proceed further, we assume that the Fermi surface is spherical. Then it can be shown that the scattering factor is given by

$$S(\underline{k}) = \sum_{mn} \frac{3j_1(k_F|\underline{R}_m-\underline{R}_n|)}{k_F|\underline{R}_m-\underline{R}_n|} \int a(\underline{r}-\underline{R}_m)\ a(\underline{r}-\underline{R}_n) \exp(i\underline{k}.\underline{r})d\underline{r}$$

$$+ \sum_n \int \sigma(\underline{r}-\underline{R}_n) \exp(i\underline{k}.\underline{r})\ d\underline{r} \qquad (3.8)$$

Then writing $\underline{R}_m-\underline{R}_n = \underline{R}$ and letting

$$\underline{r} \rightarrow \underline{r} + \frac{\underline{R}_m + \underline{R}_n}{2}$$

in the first term in equation (3.8) we find

$$S(\underline{k}) = \sum_{mn} \frac{3j_1(k_F R)}{k_F R} \exp\left[i\underline{k}.\frac{(\underline{R}_m + \underline{R}_n)}{2}\right] I_{\underline{R}}(\underline{k})$$

$$+ \sum_n \exp(i\underline{k}.\underline{R}_n)\ f_c(\underline{k}) \qquad (3.9)$$

where

$$I_{\underline{R}} = \int_\Omega a(\underline{r}-\frac{\underline{R}}{2})\ a(r+\frac{\underline{R}}{2}) \exp(i\underline{k}.\underline{r})d\underline{r} \qquad (3.10)$$

$$f_c(\underline{k}) = \int_{\Omega} \sigma(\underline{r}) \exp(i\underline{k}.\underline{r}) d\underline{r} \qquad (3.11)$$

and Ω is the atomic volume. Since,

$$\sum_n \exp(i\underline{k}.\underline{R}_n) = \sum_i \exp(i\underline{G}.\underline{R}_i)\ \delta(\underline{k}-\underline{G}) \qquad (3.12)$$

where $\underline{G}$ are the reciprocal lattice vectors and $\underline{R}_i$ is the position of the i^{th} basis atom in a unit cell, the scattering factors are only defined at the reciprocal lattice vectors:

$$S(\underline{G}) = S_o(\underline{G}) \left[\sum_n \exp\left(\frac{i\underline{G}.\underline{R}_n}{2}\right) \frac{3j_1(k_F R_n)}{k_F R_n} I_{\underline{R}_n}(\underline{G}) + f_c(\underline{G})\right] \qquad (3.13)$$

where the geometrical structure factors of the lattice are defined by

$$S_o(\underline{G}) = \sum_i \exp(i\underline{G}.\underline{R}_i) \qquad (3.14)$$

Now we can write

$$\sum_n = \sum_{R_n} \sum_{i(\text{equal } R_n)}$$

where $\sum_{i(\text{equal } R_n)}$ is that part of $\sum_n$ such that $|R_n|$ is a constant and $\sum_{R_n}$ is the sum over all shells of atoms distance R_n from some central atom. Then, defining $I_{R_n}(\underline{G})$ to be the average of $I_{\underline{R}_i}(\underline{G})$ over all $\underline{R}_i$ with $|R_i| = R_n$, we can write equation (3.13) in the form

$$S(\underline{G}) = [f_c(\underline{G}) + f_o(\underline{G})]\ S_o(\underline{G}) + \sum_{\substack{\text{all superlattices} \\ \text{labelled by n}}} f_n(\underline{G})\, S_n(\underline{G}) \qquad (3.15)$$

where

$$S_n(\underline{G}) = \sum_{ni} \exp\left[i\underline{G}.\left[\underline{R}_i + \frac{\underline{R}_n}{2}\right]\right] \qquad (3.16)$$

define the geometrical structure factors of the n^{th} super-

lattice, and

$$f_n(\underline{G}) = \frac{3j_1(k_F R_n)}{k_F R_n} \; I_{R_n}(\underline{G}) \qquad (3.17)$$

are the form factors of the scattering centres of the n^{th} superlattice.

In particular

$$f_o(\underline{G}) = \int |a(\underline{r})|^2 \exp(i\underline{G}.\underline{r}) d\underline{r} \qquad (3.18)$$

and this together with $f_c(\underline{G})$ make up the form factor of a single ion. The position vectors of the scattering centres of the superlattices are, from equation (3.16), just the mid-points of the lines joining an atom with its neighbours.

Hence, once the WF's are known, the X-ray scattering factors can be determined by use of equation (3.15). The importance of this equation is that it shows us that one centre charge distributions alone do not tell the whole story. For a full picture the two centre terms expressed by equation (3.10) have also to be considered.

§3.3 Interpretation of the X-ray Scattering Data in Solids

In the rare gas solids there are no valence electrons and hence, all the scattering comes from the core electrons. Also, since there is little or no overlap between the core electrons, the WF's in the solid will be very nearly the atomic functions. Hence, the calculated free atom scattering factors should agree with the experimental values.

Insulators and semi-conductors are characterised by a lack of conduction electrons. This corresponds to a filling up of the whole BZ. We, therefore, need not make the approximation of a spherical Fermi surface as we can sum over the occupied states exactly, namely

$$\sum_{\underline{k}<\underline{k}_F} \exp(i\underline{k}.(\underline{R}_m-\underline{R}_n)) = \sum_{\underline{k} \text{ over BZ}} \exp(i\underline{k}.(\underline{R}_m-\underline{R}_n)) = N\,\delta(\underline{R}_m-\underline{R}_n) \qquad (3.19)$$

Hence, all the superlattice terms in equation (3.15) will vanish leaving only the form factor of the ionic charge distribution. However, this one centre form factor will be in terms of the WF's, which because of overlap differ quite considerably from the free atomic wavefunctions.

In the free atomic state all degenerate levels are filled up equally and by Unsolds theorem the resulting charge density is spherically symmetric. The orthogonality of the WF's ensures that they have the symmetry of the lattice and , thus, angularity in the charge distribution, consistent with the crystal structure, is contained in the WF's. This explains why De Marco and Weiss (1965), by including angularity in the one centre charge distributions to account for sp^3 hybridization, were able to obtain agreement with the experimentally measured scattering factors of Si.

In the metals, because the valence electrons spill outside the BZ, the two centre terms in equation (3.15) are important. Hence, any calculation which considers only one-centre terms will not be in agreement with experiment. Though the sum

$$\sum_{\underline{k}<\underline{k}_F} \exp(i\underline{k}.(\underline{R}_m-\underline{R}_n))$$

cannot be calculated exactly, as shown above, the scattering factors can be approximately determined if

(i) the Fermi surface can be approximated by a spherical surface.

(ii) the WF's are known.

We have made such a calculation for Be and this is presented in the next chapter.

The difficulty in obtaining the WF's in metals prompted us to simplify equation (3.15) into a useful form, so that we may obtain information on the charge density in the transition metals by examining the experimentally determined X-ray scattering factors.

Stenhouse et al. (1977) calculated the scattering fac-

tors of Si using a bond charge model. In this model, spherical charge distributions were placed at the ionic centres and midway between nearest neighbours representing the bonding charge, such that the charge density in LCAO theory was well reproduced. The success of this model and that of De Marco and Weiss (1965) suggests that the angularity in the one centre terms can be represented by bond charges. Hence, the first term in equation (3.15) can be written in the form

$$f_o(\underline{G})\, s_o(\underline{G}) \simeq f_c^{\,c}(\underline{G})\, s_o(\underline{G}) + \sum_{\substack{\text{all superlattices} \\ \text{labelled by n}}} f_n^{\,b}(\underline{G})\, s_n(\underline{G}) \qquad (3.20)$$

where $f_o^{\,c}(\underline{G})$ and $f_n^{\,b}(\underline{G})$ are the form factors of the charges (which need not be spherical) at the ion and bond sites respectively.

Then substituting equation (3.20) into equation (3.15) we obtain an approximate formula for the scattering factor:

$$S(G) = F_o(G)\, s_o(G) + \sum_{\substack{\text{all superlattices} \\ \text{labelled by n}}} F_n(\underline{G}) s_n(\underline{G}) \qquad (3.21)$$

where

$$F_o(\underline{G}) = f_c(\underline{G}) + f_o^{\,c}(\underline{G}) \qquad (3.22)$$

is the form factor of the ionic distribution, and

$$F_n(\underline{G}) = f_n^{\,b}(\underline{G}) + f_n(\underline{G}) \qquad (3.23)$$

represent the form factors of the bond charges.

The size of the bonding charge form factors depend on the amount of overlap of the wavefunctions centred on different sites. As the d electrons, unlike the s electrons, are very localized, the only overlaps that would contribute significantly to the form factors are those arising from the hybridized s-d states.

Since the next nearest neighbour is not much further than the nearest neighbour, any analysis of the scattering factors of a b.c.c. transition metal must include at least the first two superlattice form factors. Then, writing equation (3.21) explicitly, we have

$$S(\underline{G}) = F_o(\underline{G}) \sum_i \exp(-i\underline{G}.\underline{R}_i) + F_1(\underline{G}) \sum_i \exp(-i\underline{G}.\underline{S}_i) + F_2(\underline{G}) \sum_i \exp(-i\underline{G}.\underline{T}_i) \qquad (3.24)$$

where $\underline{R}_i$ is the position vector of each basis atom and $\underline{S}_i$ and $\underline{T}_i$ are the position vectors of the scattering centres of the first two superlattices in the unit cell. Thus the scattering factors at the first five reflections are

$$\begin{aligned} S(100) &= 2F_o - 2F_2 \\ S(200) &= 2F_o - 8F_1 + 6F_2 \\ S(211) &= 2F_o - 2F_2 \\ S(220) &= 2F_o + 8F_1 + 6F_2 \\ S(310) &= 2F_o - 2F_2 \end{aligned} \qquad (3.25)$$

It is clear that $2F_o$ will be the scattering factor of the free atom and that F_1 and F_2 will be the fourier transforms of the products of hybrid orbitals centred on neighbouring sites. Assuming Slater type orbitals for the s and d functions, we see that the bond charges can be represented by exponentially decaying or Gaussian type functions centred at the bond centre. The fourier transforms of such functions will also be decaying functions, with a maximum at G = 0, and will be positive, at least for small G.

The scattering factors of Fe have been measured by Batterman et al. (1960) and by Paakari and Suortti (1967). Their results together with the Hartree-Fock free atom calculations for the first five reflections are shown in table 3.1. It now appears that Batterman et al. did not take proper account of extinction effects in their analysis of the scattering intensities. The deviation of their results from the free atom calculations are, however, confirmed

TABLE 3.1

Absolute experimental and theoretical atomic scattering for Fe.

hkl	sin θ/λ	$f_{expt.}$ (a)	f_{th} (free atom)
110	0.247	18.19	18.51
200	0.349	15.19±0.08	15.27
211	0.427	13.01±0.08	13.13
220	0.493	11.60±0.05	11.61
310	0.551	10.47±0.05	10.49

(a) Paakari and Suortti (1967)

although to a lesser degree, by Paakari and Suortti. The latter also found the deviation to be negligible beyond the fifth reflection.

From equation (3.25), we see that the deviation between the experimental and free atom calculated values can be accounted for solely by the second superlattice bond charge. We have, therefore, plotted these, from the measurements of Paakari and Suortti, against $\sin\theta/\lambda = G/4\pi$ in figure 3.1. Although the errors are quite large, we can easily fit a smooth curve through the data as would be required if the bond charge model were a good description of the electronic states in Fe. Extrapolating the contributions of F_o and F_2 $S[200]$ and $S[220]$ from table 3.1 and figure 3.1, and substituting them into equation (3.9), we find that $F_1(\kappa)$ is more localised and smaller than $F_2(k)$. This means that the charge distribution around the first neighbour bond centre is less localised and less important than that around the next nearest neighbour bond centre. This is consistent with the fact that the real space volume is greater in the [100] direction interstitial site than in the [111] one.

§3.4 Discussion

Although we have only considered Fe, the scattering factors of the other b.c.c. transition metals also show a marked discrepancy between the experimental and free atom values. Cooper's (1964) experiment on Cr also gave large discrepancies but like that of Batterman et al. on Fe is probably in error due to incorrect extinction corrections. Recent experiments of V (Mazzone and Diana 1978, Korhonen, 1971) have shown the discrepancy at the first reflection is comparable to that of Fe, so we can have confidence in results of Paakari and Suortti.

Weiss (1978) attempted to resolve this discrepancy in the b.c.c. metals by contracting the 3d triply degenerate radial wavefunctions, which point to the nearest neighbours and expanding the 3d doubly degenerate radial wavefunctions,

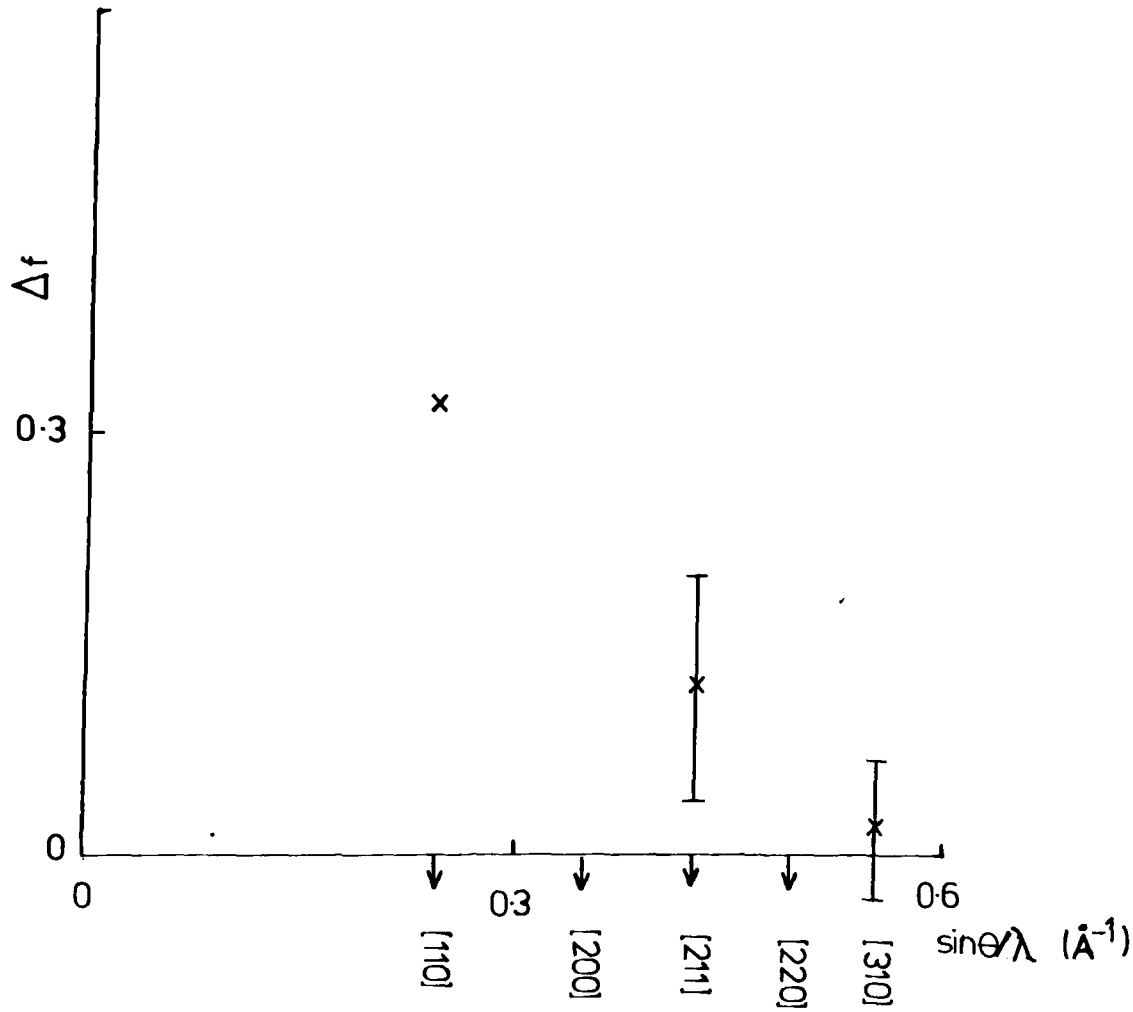

Figure 3.1

Difference in Hartree-Fock and experimental (Paakari and Suortti 1967) scattering factors, Δf, in Fe.

which point to the second nearest neighbours.

However, he had only partial success as some discrepancy between the calculated and experimental values of the [110] scattering factor of V remains. According to our formulation of the scattering factors, his model only adds angularity to the one centre terms and does not consider the two centre ones. The remaining discrepancy is, therefore, due to these two centre contributions.

This discrepancy between experimental and free atom scattering factors is also found in the f.c.c. transition metals, although it is smaller and is finite only for small G. By a similar analysis to that performed in §3.3, we can show these discrepancies are also attributable to the bond charges. The localisation of the form factors of the bonding charges in the f.c.c. metals is indicative of delocalised bonding electrons.

The present approach will not be favourable when the WF's are long range, because then one needs to consider the overlaps between many centres. It will be best for crystals in which even the valence electrons can be described by the tight binding approximation. In the transition metals, if we assume only overlaps between the hybridised orbitals, we need only consider overlaps upto the second nearest neighbour. Beyond that, the size of the overlaps are negligible.

The experimentally determined X-ray scattering factors then tell us that the bonding charges are included in the WF description and, thus, there is no conflict between the "band" picture and that based on chemical bonding. Further, it appears that bonding is less prevalent in the f.c.c. metals than in the b.c.c. metals, justifying our approximation in Chapter 2. From our analysis of the scattering factors we find that second neighbour bonding is more important than nearest neighbour bonding in the b.c.c. transition metals, resulting in a localisation of electrons in the [100] interstitial site. This is consistent with Weiss who extended the radial distribution along the next nearest neighbour direction and contracted it along the nearest

neighbour direction.

The electronic charge distribution in the b.c.c. transition metals can, therefore, approximately be written in the form:

$$\rho(\underline{r}) = \sum_i \Delta_{ion}\,(\underline{r}-\underline{R}_i) + \sum_i \Delta_{bond\ 1}\,(\underline{r}-\underline{S}_i) + \sum_i \Delta_{bond\ 2}\,(\underline{r}-\underline{T}_i) \qquad (3.26)$$

where $\underline{R}_i$, $\underline{S}_i$ and $\underline{T}_i$ have the same meaning as in equation (3.24) and Δ_{ion}, $\Delta_{bond\ 1}$, and $\Delta_{bond\ 2}$ refer to the ionic, nearest and next nearest neighbour bond charges respectively. We have used this model to calculate the phonon frequencies of Fe in Chapter 5.

CHAPTER 4

X-ray Scattering in Be

§4.1 Introduction

In the last chapter, we saw that the WF description of the valence electrons was very useful in understanding the measured X-ray scattering factors in crystals. Since the scattering factor, in this formalism, is written as a sum of fourier transforms of the overlaps of the WF's centred on different lattice sites, the expression is quickly convergent only if the WF's are short-range. Hence, this approach is best for those crystals in which the valence electrons are best described by tight-binding wavefunctions. However, the big problem is then, in spite of the value of the formalism, the practical calculation of the WF's.

To make a quantitative test of our expression for the scattering factors we have chosen h.c.p. Be. This choice is based on the following considerations:

(i) the valence electrons of Be as calculated by Donovan (1952), appear to be tight-binding in nature. Brown (1972) in her analysis of the scattering factors also arrived at the same conclusion.

(ii) the tightbinding nature of the valence electrons and the small core render it possible to obtain useful approximations of the WF's.

(iii) Inoue and Yamashita (1973) in an APW calculation on Be estimated that both the lattice parameters, c and a, in the h.c.p. lattice would have to be increased by over 160% before it became insulating. This implies an appreciable overlap between the 2s and 2p bands in the metallic phase at atmospheric pressure, which will result in substantial hybridization between these bands.

(iv) Hybridization leads to greater overlap and thus, corrections to the full BZ scattering factor are not negligible.

(v) the X-ray results of Brown (1972) indicate substantial angularity in the charge distribution.

Altmann et al. (1957) proposed that the geometrical crystal structures of the d-band metals are related to the formation of hybrids consistent with these structures. Yang and Coppens (1978) extended this idea and suggested that hybrids which have the crystal symmetry are also present in h.c.p. Be. By applying group theoretical techniques it can be shown that in the h.c.p. structure, the sp^2 (s, p_x, p_y) trigonal hybrids account for next nearest neighbour planar bonding and the sp (s, p_z) linear hybrids for nearest neighbour interplanar bonding. The charge density distribution maps are also found to be consistent with this bonding scheme (Yang and Coppens, 1978).

In h.c.p. Be the c/a ratio is much less than that of the ideal h.c.p. lattice. With the above bonding scheme, we see that this indicates stronger interplanar bonding than that within the planar layers, which is consistent with the results of Brown (1972).

In our attempt to calculate the scattering factors of Be, we have made the following assumptions and observations:

a) The valence band is a mixed s-p band.

b) sp^2 bonding is so much less prevalent than sp bonding that it can be neglected. This is very helpful in the construction of the WF's.

c) The linear sp hybrids can be shown to form the orthonormal set

$$\frac{1}{\sqrt{2}}(s + p_z) \quad \text{and} \quad \frac{1}{\sqrt{2}}(s - p_z)$$

which we assume to be equally populated. s and p_z refer to the 2s orbital and z component of the 2p orbital respectively, where z is taken to be perpendicular to the hexagonal plane.

d) The p_x and p_y bands are unoccupied. As the number of Bloch waves is equal the number of WF bands, the sp band has, therefore, four WF's of which only two are occupied.

In the next section we define WF's in a complex lattice and then modify the expression for $S(\underline{G})$ for a h.c.p. lattice appropriately. By making use of the above assump-

tions, WF's are then constructed for Be in §4.3.

In §4.4 we report the calculated scattering factors of Be and compare them with the experimental results. The validity of certain approximations that we have made and the actual results are discussed in §4.5.

§4.2 Wannier Functions and Scattering Factors in Complex Lattices

Complex lattices are those lattices in which the unit cell contains more than one atom. Then, by analogy, we define

$$\psi_{\alpha\underline{k}}(\underline{r}) = \frac{1}{\sqrt{(Ns)}} \sum_{\mu} \exp(i\underline{k}.\underline{R}_{\mu})\, a_{\alpha}(\underline{r}-\underline{R}_{\mu}) \qquad (4.1)$$

and

$$a_{\alpha}(\underline{r}-\underline{R}_{\mu}) = \frac{1}{\sqrt{(Ns)}} \sum_{\underline{k}} \exp(-i\underline{k}.\underline{R}_{\mu})\, \psi_{\alpha\underline{k}}(\underline{r}) \qquad (4.2)$$

These functions now satisfy all the usual orthonormality conditions which have to be obeyed by Bloch functions and WF's.

In Be there are two atoms per unit cell and so we can consider the cell to be a mesh of two sublattices. If we denote the position vectors of the atoms of one sublattice by $\underline{R}_n$, those of the other can be denoted by $\underline{R}_n + \underline{d}$. Because both atoms are related through a centre of inversion, it is convenient to choose local axes x, y and z on the second atom inverted with respect to those on the first. Then, if the WF's centred on the atoms of one sublattice are denoted by $a(\underline{r} - \underline{R}_n)$, the WF's centred on the atoms of the other sublattice will be $a(\underline{R}_n + \underline{d} - \underline{r})$

Hence, omitting the band index, from equation (4.1) the Bloch function is given by

$$\psi_{\underline{k}}(\underline{r}) = \frac{1}{\sqrt{(Ns)}} \sum_{n} \{a(\underline{r}-\underline{R}_n) + a(\underline{R}_n+\underline{d}-\underline{r})\exp(i\underline{k}.\underline{d})\}\exp(i\underline{k}.\underline{R}_n) \qquad (4.3)$$

Then, by a similar analysis to that carried out in §3.2, we find that the structure factor can be written in the form

$$S(\underline{k}) = \sum_{\alpha\beta} \sum_{\underline{k}mn} \exp(i\underline{k}.(\underline{R}_m-\underline{R}_n)) \int a_\alpha(\underline{r}-\underline{R}_n)a_\beta(\underline{r}-\underline{R}_m)\exp(i\underline{k}.\underline{r})d\underline{r}$$

$$+ \sum_{\alpha\beta} \sum_{\underline{k}mn} \exp(i\underline{k}.(\underline{R}_m-\underline{R}_n)) \int a_\alpha(\underline{R}_n+\underline{d}-\underline{r})a_\beta(\underline{R}_m+\underline{d}-\underline{r})\exp(i\underline{k}.\underline{r})d\underline{r}$$

$$+ \sum_{\alpha\beta} \sum_{\underline{k}mn} \exp(i\underline{k}.(\underline{R}_m-\underline{R}_n)) \int a_\alpha(\underline{r}-\underline{R}_m)a_\beta(\underline{R}_n+\underline{d}-\underline{r})\exp(i\underline{k}.\underline{r})d\underline{r}$$

$$+ \sum_{\alpha\beta} \sum_{\underline{k}mn} \exp(i\underline{k}.(\underline{R}_m-\underline{R}_n)) \int a_\alpha(\underline{r}-\underline{R}_n)a_\beta(\underline{R}_m+\underline{d}-\underline{r})\exp(i\underline{k}.\underline{r})d\underline{r} \qquad (4.4)$$

where α and β refer to the $(s + p_z)$ and $(s - p_z)$ bands respectively.

We now make the following substitutions in equation (4.4)

(i) In the first sum $\underline{r} \to \underline{r} + \frac{\underline{R}_m + \underline{R}_n}{2}$

(ii) In the second sum $\underline{r} \to \underline{r} + \frac{\underline{R}_m + \underline{R}_n + 2\underline{d}}{2}$

(iii) In the third and fourth sums $\underline{r} \to \underline{r} + \frac{\underline{R}_m + \underline{R}_n + \underline{d}}{2}$

Then, it follows that the scattering factors are zero except at the reciprocal lattice vectors, where they are given by the expression

$$S(\underline{G}) = \left| \sum_{\alpha\beta n} \frac{3j_1(k_F R_n)}{k_F R_n} \sum_{\underline{f}} \exp(-i\underline{G}.(\frac{\underline{R}_n}{2} + \underline{f}))\ I_{\alpha\beta}(\underline{R}_n,\underline{G}) \right.$$

$$\left. + \sum_{\alpha\beta n} \frac{3j_1(k_F R_n')}{k_F R_n'} \sum_{\underline{f}} \exp(-i\underline{G}.(\frac{\underline{R}_n'}{2} + \underline{f}))\ I_{\alpha\beta}(\underline{R}_n',\underline{G}) \right| \qquad (4.5)$$

where

$$\underline{R}_n' = \underline{R}_n + \underline{d}$$

and $\underline{f}$ are the position vectors of the atoms in the sublattice. For Be, $\underline{f} = 0$ or $\underline{d}$.

The overlap integrals $I(\underline{R}_n,\underline{G})$ and $I(\underline{R}_n',\underline{G})$ are defined by the equations

$$I_{\alpha\beta}(\underline{R}_n,\underline{G}) = \int a_\alpha(\underline{r}-\frac{\underline{R}_n}{2})\, a_\beta(\underline{r}+\frac{\underline{R}_n}{2}) \exp(i\underline{G}.\underline{r})d\underline{r} \quad (4.6)$$

which is the fourier transform of the overlap between functions centred on atoms of the same sublattice, and

$$I_{\alpha\beta}(\underline{R}_n',\underline{G}) = \int a_\alpha(\underline{r}-\frac{\underline{R}_n'}{2})\, a_\beta(\frac{-\underline{R}_n'}{2}-\underline{r}) \exp(i\underline{G}.\underline{r})d\underline{r} \quad (4.7)$$

which is the fourier transform of the overlap between functions centred on atoms of different sublattices.

§4.3 Construction of the Wannier Functions

As mentioned in the Introduction to this Chapter, we can construct approximate WF's for Be because of the tight binding nature of the valence electrons. Comparing the tight binding Bloch function to that given by equation (4.3) we see that a first order approximation of the WF's are in fact the atomic orbitals. However, due to the orthogonality property of the WF's, the atomic orbitals have to be made orthogonal to each other.

In Be we assume only two occupied bands. If we denote the $(s + p_z)$ atomic orbital centred on $\underline{R}_n$ by $\psi_1(\underline{r}-\underline{R}_n)$ and the corresponding $(s - p_z)$ atomic orbital by $\psi_2(\underline{r}-\underline{R}_n)$ then

$$\underline{\underline{\Delta}}_{ij}(m,n) = \int \psi_i(\underline{r}-\underline{R}_m)\, \psi_j(\underline{r}-\underline{R}_n)\, d\underline{r} \quad (4.8)$$

is the $(i + m)$ by $(j + n)$ overlap matrix between these functions centred on different lattice sites.

If the ψ's are WF's, we require

$$\underline{\Delta}_{ij}(m,n) = \delta_{ij}\,\delta_{mn} \qquad (4.9)$$

To satisfy equation (4.9), we need to orthogonalise the ψ's. We transform the set $\{\psi(\underline{r}-\underline{R}_m)\}_i$ to an orthogonal set $\{W(\underline{r}-\underline{R}_m)\}_i$ by the symmetric orthogonalization procedure introduced by Löwdin (1956).

It can be shown that the complete orthogonal sets can be written in terms of the non-orthogonal atomic functions, nemely

$$W_1(\underline{r}-\underline{R}_m) = \underline{\Delta}_{11}^{-1/2}\,\psi_1(\underline{r}-\underline{R}_m) \qquad (4.10)$$

and

$$W_2(\underline{r}-\underline{R}_m) = \frac{\underline{\Delta}_{22}^{-1/2}(\psi_2(\underline{r}-\underline{R}_m) - \underline{\Delta}_{11}^{-1}\,\underline{\Delta}_{12}\psi_1(\underline{r}-\underline{R}_m))}{(1 - \underline{\Delta}_{11}^{-1}\,\underline{\Delta}_{22}^{-1}\,\underline{\Delta}_{21}\,\underline{\Delta}_{12})} \qquad (4.11)$$

where $\underline{\Delta}_{11}$, $\underline{\Delta}_{12}$, $\underline{\Delta}_{21}$ and $\underline{\Delta}_{22}$ are the matrices making up the block overlap matrix $\underline{\Delta}_{ij}(m,n) \equiv \underline{\Delta}$. From equations (4.8) and and (4.9) we see that for the WF's to be exact the $\underline{\Delta}$ matrices are infinite. This is equivalent to saying that the WF on one lattice site is orthogonal to WF's on all other lattice sites. This is of course not practical in any calculation. The accuracy of the constructed WF's is, therefore, dependent on:

(i) the order to which the $\underline{\Delta}_{ij}$ matrices are taken;

(ii) the order to which the inverses and products in equations (4.10) and (4.11) are calculated; and

(iii) the size of the elements of the $\underline{\Delta}$ matrices.

Hence, equations (4.10), (4.11) and (4.8) provide the basis of an approximate calculation of the WF's.

§4.4 Calculation of the X-ray Scattering Factors in Be

Be has a h.c.p. crystal structure with lattice parameters a = 2.2858Å and c = 3.5843Å. In the calculation of

of the WF's we require the atomic 2s and 2p orbitals, which, for our calculations, we have taken to be the orthogonalized Slater-type analytic functions given by Duncanson and Coulson (1944). The screening parameter of the 2p orbital was extrapolated from that given for the heavier elements.

The normalised hybrid wavefunctions then are

$$\psi_1(\underline{r}) = \frac{1}{\sqrt{2}} (Ar \exp(-\mu r) - B \exp(-\nu r) + Cz \exp(-\lambda r)) \tag{4.12}$$

$$\psi_2(\underline{r}) = \frac{1}{\sqrt{2}} (Ar \exp(-\mu r) - B \exp(-\nu r) - Cz \exp(-\lambda r)) \tag{4.13}$$

where the constants are given in table 4.1.

Since the only hybrids we allow in this system are the $(s \pm p_z)$ hybrids, we need only consider the overlaps between the wavefunctions centred on one atom and its neighbours up to and including the third shell. This corresponds to taking its first fourteen neighbours.

For the $(s \pm p_z)$ hybrid orbitals the overlap matrices defined in §4.3 can be written in terms of the following six overlaps:

$$\sigma_1 = \int \psi_1(\underline{r})\, \psi_1(\underline{r}-\underline{R}_2)d\underline{r} = \int \psi_2(\underline{r})\, \psi_2(\underline{r}-\underline{R}_5)d\underline{r}$$

$$\sigma_2 = \int \psi_1(\underline{r})\, \psi_1(\underline{r}-\underline{R}_8)d\underline{r} = \int \psi_2(\underline{r})\, \psi_2(\underline{r}-\underline{R}_8)d\underline{r}$$

$$\sigma_3 = \int \psi_1(\underline{r})\, \psi_1(\underline{r}-\underline{R}_{14})dr = \int \psi_2(\underline{r})\, \psi_2(\underline{r}-\underline{R}_{15})d\underline{r}$$

$$\sigma_4 = \int \psi_1(\underline{r})\, \psi_2(\underline{r}-\underline{R}_2)d\underline{r} = \int \psi_2(\underline{r})\, \psi_1(\underline{r}-\underline{R}_s)d\underline{r}$$

$$\sigma_5 = \int \psi_1(\underline{r})\, \psi_2(\underline{r}-\underline{R}_8)d\underline{r} = \int \psi_2(\underline{r})\, \psi_1(\underline{r}-\underline{R}_8)d\underline{r}$$

$$\sigma_6 = \int \psi_1(\underline{r})\, \psi_2(\underline{r}-\underline{R}_{14})d\underline{r} = \int \psi_2(\underline{r})\, \psi_1(r-R_{15})d\underline{r}$$

where $\underline{R}_n$ are the position vectors of the atoms labelled by n relative to the 'zero' atom labelled 1. From the spatial

TABLE 4.1

Parameters of 2s and 2p wavefunctions of Be.

Parameter	Value
A ($\text{Å}^{-5/2}$)	0.837
B ($\text{Å}^{-3/2}$)	1.788
C ($\text{Å}^{-5/2}$)	1.128
μ (Å^{-1})	1.851
ν (Å^{-1})	6.200
λ (Å^{-1})	1.701

extent of the hybrid orbitals, it is clear that all other overlaps will be much smaller and hence, can be neglected.

Using the functions given in equations (4.12) and (4.13), we have calculated these overlaps and they are presented in table 4.2. From their definition, it follows that

$$\underline{\underline{\Delta}}_{11} = \underline{\underline{\Delta}}_{22}$$

and

$$\underline{\underline{\Delta}}_{21} = \underline{\underline{\Delta}}_{12}^{\dagger}$$

where the dagger † denotes the hermitian conjugate. For the system of fifteen atoms considered, we can express the $\underline{\underline{\Delta}}$ matrices as

$$\underline{\underline{\Delta}}_{11} = \underline{\underline{1}} + \underline{\underline{S}} \tag{4.15}$$

and

$$\underline{\underline{\Delta}}_{12} = \underline{\underline{T}}$$

where $\underline{\underline{S}}$ and $\underline{\underline{T}}$ depend on the σ_i(i = 1 to 6).

Due to the complexity of the $\underline{\underline{S}}$ and $\underline{\underline{T}}$ matrices, we have worked only to order $\underline{\underline{ST}}$ and $\underline{\underline{TT}}^{\dagger}$ in the expansion for the approximate WF's from equations (4.10) and (4.11). The validity of this approximation is discussed in the next section.

It may be easily shown that

$$W_1(\underline{r}) = \psi_1(\underline{r}) - \frac{\sigma_1}{2}(\xi_1(\underline{r}) + \eta_1(\underline{r})) - \frac{\sigma_2}{2}\zeta_1(\underline{r}) - \frac{\sigma_3}{2}(\psi_1(\underline{r}-\underline{R}_{14}) + \psi_1(\underline{r}-\underline{R}_{15})) \tag{4.17}$$

and

TABLE 4.2

Overlap values

Type of Overlap	Value
σ_1	0.184
σ_2	0.370
σ_3	-0.058
σ_4	0.638
σ_5	0.052
σ_6	0.408

$$W_2(\underline{r}) = \left(1 + \frac{3\sigma_4^2 + 6\sigma_5^2 + \sigma_6^2}{2}\right) \psi_2(\underline{r})$$

$$+ \tfrac{1}{2}\,(2\sigma_4\sigma_5 + \sigma_4\sigma_6 - \sigma_1)(\xi_2(\underline{r}) + \eta_2(\underline{r}))$$

$$+ \tfrac{1}{2}\,(\sigma_4^2 + 2\sigma_5^2 - \sigma_2)\,\zeta_2(\underline{r}) - \frac{\sigma_3}{2}\,(\psi_2(\underline{r}-\underline{R}_{14}) + \psi_2(\underline{r}-\underline{R}_{15}))$$

$$+ \frac{3}{2}\,(3\sigma_1\sigma_4 + 6\sigma_2\sigma_5 + \sigma_3\sigma_6)\,\psi_1(\underline{r}) + \frac{3}{2}(2\sigma_1\sigma_5 + \sigma_3\sigma_4)\xi_1(\underline{r})$$

$$+ (\tfrac{3}{2}(\sigma_1\sigma_6 + 2\sigma_1\sigma_5 + 2\sigma_2\sigma_4) - \sigma_4)\,\eta_1(\underline{r})$$

$$+ (\tfrac{3}{2}(\sigma_1\sigma_4 + 2\sigma_2\sigma_5) - \sigma_5)\,\zeta_1(\underline{r})$$

$$+ (\tfrac{9}{2}\,\sigma_1\sigma_4 - \sigma_6)\,\psi_1(\underline{r}-\underline{R}_{15}) \qquad (4.18)$$

where

$$\xi_i = \sum_{n=2}^{4} \psi_i\,(\underline{r}-\underline{R}_n)$$

$$\eta_i = \sum_{n=5}^{7} \psi_i\,(\underline{r}-\underline{R}_n)$$

and

$$\zeta_1 = \sum_{n=8}^{13} \psi_i\,(\underline{r}-\underline{R}_n)$$

Since we have only considered overlaps up to and including the third shell of neighbours, we need consider only the first three superlattice contributions to the scattering factor in equation (4.5). The scattering factor at the reciprocal lattice vectors, defined by Miller indices $[\underline{hkl}]$, is then

$$S[\underline{hkl}] = \Big| s_o[\underline{hkl}] \sum_{\alpha\beta} I_{\alpha\beta}(0,hkl)$$

$$+ \frac{3j_1(k_F d)}{k_F d}\, s_1[\underline{hkl}] \sum_{\alpha\beta} \overline{I_{\alpha\beta}(d,hkl)}$$

$$+ \frac{3j_1(k_F a)}{k_F a} S_2[hkl] \sum_{\alpha\beta} \overline{I_{\alpha\beta}(a,hkl)}$$

$$+ \frac{3j_1(k_F c)}{k_F c} S_3[hkl] \sum_{\alpha\beta} \overline{I_{\alpha\beta}(c,hkl)} \Bigg| \qquad (4.19)$$

where $S_n[hkl]$ is the geometrical structure factor of the n^{th} superlattice, $\overline{I_{\alpha\beta}(x,hkl)}$ are the average overlap integrals defined by equations (4.6) and (4.7) over $\underline{R}_n$ and $\underline{R}_n'$ with moduli x, and d, a and c are the first, second and third neighbour shell distances respectively.

The X-ray scattering factors of Be as measured by Brown show considerable disagreement with the free atom calculations (Weiss 1968). The discrepancies between the two sets are largest at the first five observed reflections. We have, therefore, calculated $S(\underline{G})$ from equation (4.19) at these reciprocal lattice vectors.

The WF's were constructed by the method described in §4.3. These were then used in equations (4.6) and (4.7) to evaluate the average overlap integrals of equation (4.19). Implicit in equation (4.19) is the fact that we have used a spherical Fermi surface approximation. The validity of this approximation is also discussed in the next section.

The calculated scattering factors are tabulated in table 4.3, together with the experimentally determined values of Brown. Also shown are those calculated by Brown using a tight binding approach, and the free atom core and valence electron contributions.

§4.5 Discussion

Before discussing the results of our calculations which are presented in table 4.3, we make a few comments on the two major approximations, other than the assumptions of the model, that we have used in the calculations.

TABLE 4.3

Comparison of theoretical and experimental structure factors for Be.

G(hkl)	core ($1s^2$) contribution	valence contribution	S(G) present calculation	S(G) (a) experimental	S(G) (a) Brown's calculation
100	1.739	0.141	1.878	1.715	1.720
002	3.371	-0.400	2.971	2.978	3.038
101	2.886	-0.089	2.797	2.606	2.798
102	1.475	-0.100	1.375	1.403	1.408
110	2.668	-0.073	2.595	2.502	2.621

(a) Brown (1972).

The WF's used to calculate the structure factors were obtained by:

(i) orthogonalizing the hybrid orbitals on one atom with only the first three shells of neighbours;

(ii) truncating the resulting expressions to order $\underline{\underline{S}}\underline{\underline{T}}$ and $\underline{\underline{T}}^{+}\underline{\underline{T}}$ of the overlap matrices.

Both these approximations lead to an error in the long range part of the WF. The first term in equation (4.19) is just the fourier transform of the square of the WF. Any errors in the long range part of the WF will, therefore, only show itself at small G, the largest error being at G = 0. We estimate that even at the first reflection, $\underline{G}$ is sufficiently large to minimize the errors which are of order 1/Gr where r is the interatomic spacing. The other terms in equation (4.19) are essentially the fourier transforms of symmetric functions centred away from the origin. Hence, once again the errors in the WF's will not lead to any significant errors in the scattering factors away from G = 0. So, although we can make no claims on the accuracy of the calculated WF's the approximations used in obtaining them appear to useful in the calculation of the X-ray scattering factors.

The other major approximation we have made is that of a spherical Fermi surface. In Be, this is not a good approximation. As we saw in Chapter 3, the first term in equation (4.19) is that which would be obtained for an insulator, i.e. one with a filled BZ and where the angularity in the charge distribution is incorporated into the WF. Be is a very good example of a compensated metal and so the other terms in equation (4.19) are just those contributions arising from the holes in the first BZ, and from the electrons outside this zone. The approximation we have made, therefore entails describing these electron and hole states by hybrid wavefunctions with $|\underline{k}| = k_F$. In doing this, we are of course giving it more weight than is due because, in addition to the hybrid states, there exists at this wave-vector free electron like states which will contribute differently to the scattering. We have followed the above approach and not used plane waves for the following reasons:

(i) plane waves (including standing waves) have

fixed values of $\underline{k}$ and are hence spatially spread over the whole volume in real space. This does not take account of the fact that these states must be excluded from the core regions.

(ii) the overlap electrons with energy near E_f will not be properly represented.

(iii) to find its correct contribution to the scattering factors, we would first have to calculate the contributions from the zones into which the electrons have spilled over. In Be, this would include the second and third BZ.

From table 4.3. we see that the free atom $1s^2$ core constantly overestimates the scattering factor at all the reflections. With the exception of the first reflection, we find that the introduction of angularity, through the hybridised WF's into the core charge density and the inclusion of the overlap terms lead to smaller scattering factors than that predicted from free atom calculations. Thus, the general trend is to bring the theoretically calculated scattering factors more into agreement with experiment. Our results are also in good agreement with the tight-binding calculations of Brown. This vindicates our model with the assumption of only sp linear hybridization and shows that most of the localised charge is interplanar.

Though four of the five calculated scattering factors show excellent agreement with experiment, the one serious disagreement is at the first reflection. This is not a result of the above mentioned approximations.

If we consider a charged 'blob' model similar to that proposed in Chapter 3, we arrive at the same conclusions. In such a model, placing charges at the mid-points between an atom and its first three shells of neighbours, we find that the scattering factors at the first five reflections are given by

$$
\begin{aligned}
S(100) &= f_0 + 2f_1 - f_2 + f_3 \\
S(002) &= 2(f_0 - 3f_1 + 3f_2 + f_3) \\
S(101) &= 3(f_0 - f_2 - f_3) \\
S(102) &= f_0 - 2f_1 - f_2 + f_3 \\
S(110) &= 2(f_0 - f_1 - f_2 + f_3)
\end{aligned}
\qquad (4.20)
$$

where f_n are the form factors of the 'blobs' of the n^{th} superlattice.

Since these form factors are fourier transforms of exponential or Gaussian functions, they will be positive, at least for small G. Also, as the linear sp bonding is more prevalent than the sp^2 planar bonding, the first superlattice form factor will be greater than the second superlattice form factor. Hence, from equation (4.20) all the scattering factors, except at the first reflection, will be less than the free atom calculated ones which is in agreement with our calculations. The scattering factor at [100] will, however, be larger than the free atom result, again in agreement with our calculations. Hence, the discrepancy at [100] is not a result of the approximations made in the calculation, but something more subtle. We have not been able to find a satisfactory explanation but suggest it might be due to the fact that we did not take account of the plane wave like states in the form of othogonalized plane waves. This would give rise to a form that is finite only at small G (e.g. at the first reflection) and almost zero at large G.

The good agreement of our calculations with the experimental scattering factors at G, other than at the first reflection justifies the model that we have used and the approximations that were made. Further, it shows that the WF description of the hybrids is a useful one, and also that the bond charge model is quite realistic.

CHAPTER 5

The interatomic potential in the B.C.C. transition metals

§5.1 Introduction

By investigating the experimentally measured scattering factors of the transition metals, we saw that a useful representation of the angularity in the charge distribution could be obtained by the introduction of bond charges. A description of the outer electrons in terms of WF's leads to the concept of bonding charges situated at interstial sites. By linear response theory, these give rise to angularity in the force fields. Thus, as angular forces are necessarily required in a description of the transition metals, any model must in some way incorporate these bonding charges.

From our discussion in Chapter 3 it is clear that the angularity in the charge distribution and hence, in the force fields is greater in the b.c.c. than f.c.c. transition metals. We have, therefore, made a model for the b.c.c. transition metals from which the phonon frequencies and elastic properties may be calculated.

In our model, in addition to the ions situated at the lattice sites we place bond electrons at interstitial sites consistent with the symmetry of the crystal. The bonds are constructed in the manner proposed by Altmann et al. (1957). In this model the charge density will then be

$$\rho(\underline{r}) = \sum_n \Delta_i(\underline{r}-\underline{R}_n) + \sum_\nu \Delta_b(\underline{r}-\underline{r}_\nu) \qquad (5.1)$$

where $\underline{R}_n$ denotes the ionic positions and $\underline{r}_\nu$ the bond electron positions. Since the bond electrons are situated halfway along a bond connecting two atoms, we can write

$$\underline{r}_\nu = \frac{\underline{R}_n + \underline{R}_m}{2} \qquad (5.2)$$

As the first two superlattice form factors in Fe are sufficient to explain the X-ray scattering factor results equat-

ion (5.1) can be reduced to equation (3.26). Hence, the picture of the b.c.c. transition metal is that of ions situated at the lattice sites and bond electrons situated at the first two superlattice sites all immersed in an uniform electron gas. The ions then interact with each other directly and via the electron gas.

This interaction takes the same form as for the simple metals. However, in addition to this interaction, there are also the interactions of the bond electrons between themselves and with the ions. These interactions will also be screened by the electron gas. However, their exact nature has not been investigated.

If we denote the ion-ion, bond electron-ion and bond electron-bond electron interactions by $\emptyset_1$, $\emptyset_2$ and $\emptyset_3$ respectively, the total energy of the system can be written in the form

$$E = \tfrac{1}{2} \sum_{n \neq m} \emptyset_1(|\underline{R}_m - \underline{R}_n|) + \sum_{n\nu} \emptyset_2(|\underline{R}_n - \underline{r}_\nu|) + \tfrac{1}{2} \sum_{\nu \neq \mu} \emptyset_3(|\underline{r}_\nu - \underline{r}_\mu|) + E_v(V) \tag{5.3}$$

where the set $\{\underline{r}_\nu\}$ are completely determined by the set $\{\underline{R}_n\}$ through equation (5.2) with the condition that

$$|\underline{R}_m - \underline{R}_n| = R_c$$

where R_c is the first or second neighbour distance.

In writing this we have assumed that the bond charges are spherically symmetric about the bond centre ensuring that the bond electron-ion and bond electron-bond electron interactions are central.

In §5.2 we derive expressions for the second order elastic constants and the phonon frequencies in cubic metals with metallic binding.

These expressions are used in §5.3 to calculate the second order elastic constants and phonon frequencies of

Fe. We have chosen Fe as an example because:

(i) the X-ray scattering factors show that its charge distribution is quite angular and can be written in the form given in equation (3.26).

(ii) a liquid pair potential has been calculated by Waseda and Ohtani (1975b). This provides a starting point in the determination of $\phi_1(r)$ in equation (5.3). The liquid potential was then refined and the effects of the bond charges on the phonon examined. Because of the similarity of the Cauchy discrepancy and the phonon dispersion curves with that of K, it would appear that the forces in Fe are almost central. However, it is clear from the arguments presented in Chapter 3 that this is not the case. Hence, this similarity must be due to some cancellation between the effects of the bond charges and that of E_v. In this sense, Fe is not the best choice, but the lack of a liquid pair potential in any of the other b.c.c. transition metals has led us to make this particular choice.

In §5.4 we discuss the usefulness of the bond charge model and ways in which a correct description of the force field can be obtained. As the central pair potential gives an important contribution to the total energy, we have investigated its effects on the liquid structure factor.

§5.2 Expressions for the Elastic Constants and Phonon Frequencies

In the following derivations, we assume that the bond charges do not change appreciably under an infinitesimal deformation; hence, the potential functions ϕ_2 and ϕ_3 remain unaltered.

a) Elastic Constants for a Cubic Crystal

If there are 2J bonds pointing out from one atom, then there are J bond electrons associated with each atom with position vectors $\underline{r}^{\alpha}(\alpha = 1....J)$ relative to the atom. The bond energy per unit undeformed volume can be written in the form

$$U = \frac{1}{2\Omega_o} \sum_s \left(\phi_1(R^s) + 2 \sum_\alpha^J \phi_2(|\underline{R}^s + \underline{r}^\alpha|) + \sum_{\alpha \neq \beta}^J \phi_3(|\underline{R}^s + \underline{r}^\alpha - \underline{r}^\beta|) \right) + \varepsilon_v(V) \qquad (5.4)$$

where $\underline{R}^s$ are the position vectors of the s^{th} atom relative to some 'zero' atom and Ω_o is the undeformed atomic volume. $\varepsilon_v(V)$ is defined by equations (2.14) and (2.38).

Under a homogeneous deformation, we let

$$\underline{R}^s \rightarrow \underline{r}^s = \underline{R}^s + \underline{u}^s$$

Then adopting a similar procedure and notation to that used in Chapter 2, it can be shown that the first and second order elastic constants in a cubic crystal are

$$C_1 = \sum_s \left(\psi_1'(x^s)^2 + \sum_\alpha^J \psi_2' x^{s\alpha} x^s + \tfrac{1}{2} \sum_{\alpha \neq \beta} \psi_3' x^{s\beta} x^s \right) + \varepsilon_v' \equiv 0 \qquad (5.5)$$

$$C_{11} = \sum_s \left(\psi_1''(x^s)^4 + \tfrac{1}{2} \sum_\alpha^J \psi_2''(x^s)^2 (x^{s\alpha})^2 + \psi_2'((x^s)^2 - x^{s\alpha} x^s) + \tfrac{1}{4} \sum_{\alpha \neq \beta}^J (\psi_3''(x^s)^2 (x^{s\beta})^2 + \psi_3'((x^s)^2 - x^{s\beta} x^s)) \right) + \varepsilon_v'' - \varepsilon_v' \qquad (5.6)$$

$$C_{12} = \sum_s \left(\psi_1''(x^s)^2 (y^s)^2 + \tfrac{1}{2} \sum_\alpha^J \psi_2'' x^s y^s x^{s\alpha} y^{s\alpha} + \tfrac{1}{4} \sum_{\alpha \neq \beta}^J \psi_3'' x^s y^s x^{s\beta} y^{s\beta} \right) + \varepsilon_v'' + \varepsilon_v' \qquad (5.7)$$

and

$$C_{44} = \sum_s \left(\psi_1''(x^s)^2 (y^s)^2 + \frac{1}{8} \sum_\alpha^J 2 \left(\psi_2''((x^s)^2 (y^{s\alpha})^2 + x^s y^s x^{s\alpha} y^{s\alpha}) + \psi_2'((x^s)^2 - 2x^{s\alpha} x^s) \right) + \frac{1}{16} \sum_{\alpha \neq \beta}^J 2 \left(\psi_3''((x^s)^2 (y^{s\beta})^2 + x^s y^s x^{s\beta} y^{s\beta}) + \psi_2'((x^s)^2 - 2x^{s\beta} x^s) \right) \right) - \varepsilon_v' \qquad (5.8)$$

The Cauchy discrepancy given by

$$C_{12}-C_{44} = \frac{1}{8}\sum_{s}\Big[\sum_{\alpha}(2\psi_2''(x^s y^s x^{s\alpha} y^{s\alpha} - (x^s)^2(y^{s\alpha})^2)$$

$$+ \psi_2'(2x^{s\alpha}x^s-(x^s)^2)\Big) + \tfrac{1}{2}\sum_{\alpha\neq\beta}^{J}\Big[2\psi_3''(x^s y^s x^{s\beta} y^{s\beta}-(x^s)^2(y^{s\beta})^2)$$

$$+ \psi_3'(2x^{s\beta}x^s-(x^s)^2))\Big] + \varepsilon_v'' + 2\varepsilon_v' \qquad (5.9)$$

now contains both structure dependent and structure independent quantities. Equation (5.9) shows explicitly the angular contribution to the Cauchy discrepancy.

b) Phonon Frequencies

The phonon frequencies in this model are given by equations (2.26) to (2.28), with the potential energy given by equation (5.3).

After performing the differentiations, we find that the contribution from the structure dependent quantities to the dynamical matrix, $D^A_{\alpha\beta}(\underline{k})$ is given by

$$MD^A_{\alpha\beta}(\underline{k}) = \sum_{1'}{}' \phi_{1\alpha\beta}(r(1'))\,[\underline{1} - \exp(i\underline{k}.r(1'))]$$

$$+ \tfrac{1}{2}\sum_{1's'}{}' \phi_{2\alpha\beta}\left(\left|\frac{\underline{r}(s')}{2} - \underline{r}(1')\right|\right)[\underline{1} - \exp(i\underline{k}.r(1'))]$$

$$[\underline{r}(s')=\pm 2\tau^{\alpha}]$$

$$- \tfrac{1}{4}\sum_{1's'}{}' \phi_{2\alpha\beta}\left(\left|\frac{\underline{r}(1')}{2} - r(s)\right|\right)[\underline{1} - \exp(i\underline{k}.r(1'))]$$

$$[\underline{r}(1')=\pm 2\tau^{\alpha}]$$

$$+ \tfrac{1}{2}\sum_{1's'}{}' \phi_{2\alpha\beta}\left(\left|\frac{\underline{r}(s')+\underline{r}(1')}{2}\right|\right)[\underline{1} - \exp(i\underline{k}.\underline{r}(1'))]$$

$$[\underline{r}(s')-\underline{r}(1')=\pm 2\tau^{\alpha}] \qquad (5.10)$$

where

$$\phi_{n\alpha\beta}(\mu) = \frac{\partial^2 \phi_n(\mu)}{\partial\mu_\alpha \partial\mu_\beta}$$

Equation (5.10) together with the contribution from $E_v(V)$, given in §2.2 thus, enables us to calculate the phonon frequencies in the three symmetry directions in the bond charge model.

§5.3 Pair Potentials, Phonon Frequencies and Force Fields in Fe

The arguments presented in Chapter 2 as to why the central pair potential in the solid state can in the first instance be approximated by the liquid pair potential, remain valid in the b.c.c. transition metals. Waseda and Ohtani (1975b) measured the liquid X-ray structure factor of Fe and extracted a pair potential by the Born-Green (1946) method. The main difference between the solid and liquid pair potentials will be the way in which it falls off at large r. We have fitted the pair potential of Waseda and Ohtani to the form given by equation (2.37). The procedure was the same as that used for Ni. The hard core again characterised by a repulsivity of sixteen was influenced by the melting and liquid structure factor data.

Our interpretation of the measurements of the melting temperatures under pressure in §2.3, lead us to assume the repulsivity of Fe to be of the order of fifteen. The similarity of the long range liquid $S(\underline{k})$ of Fe and Ni reinforces our choice of n. The major difference between the solid and liquid potentials is in the mean free path, λ^{-1}. In the liquid state, due to the disorder, λ is about five times greater than in the solid. Since the nearest neighbour spacing in Fe is almost the same as in Ni, we expect the inverse mean free paths in the solid and liquid to be almost the same namely 0.05Å^{-1} and 0.20Å^{-1}.

Using the liquid potential, but with λ_{solid} as the inverse mean free path, we have calculated the phonon frequencies in b.c.c. Fe. The parameters in the potential were adjusted until the best fit to the experimentally determined phonon frequencies, which is shown in figure 5.1, was obtained. The resulting central ion-ion pair potential was given by

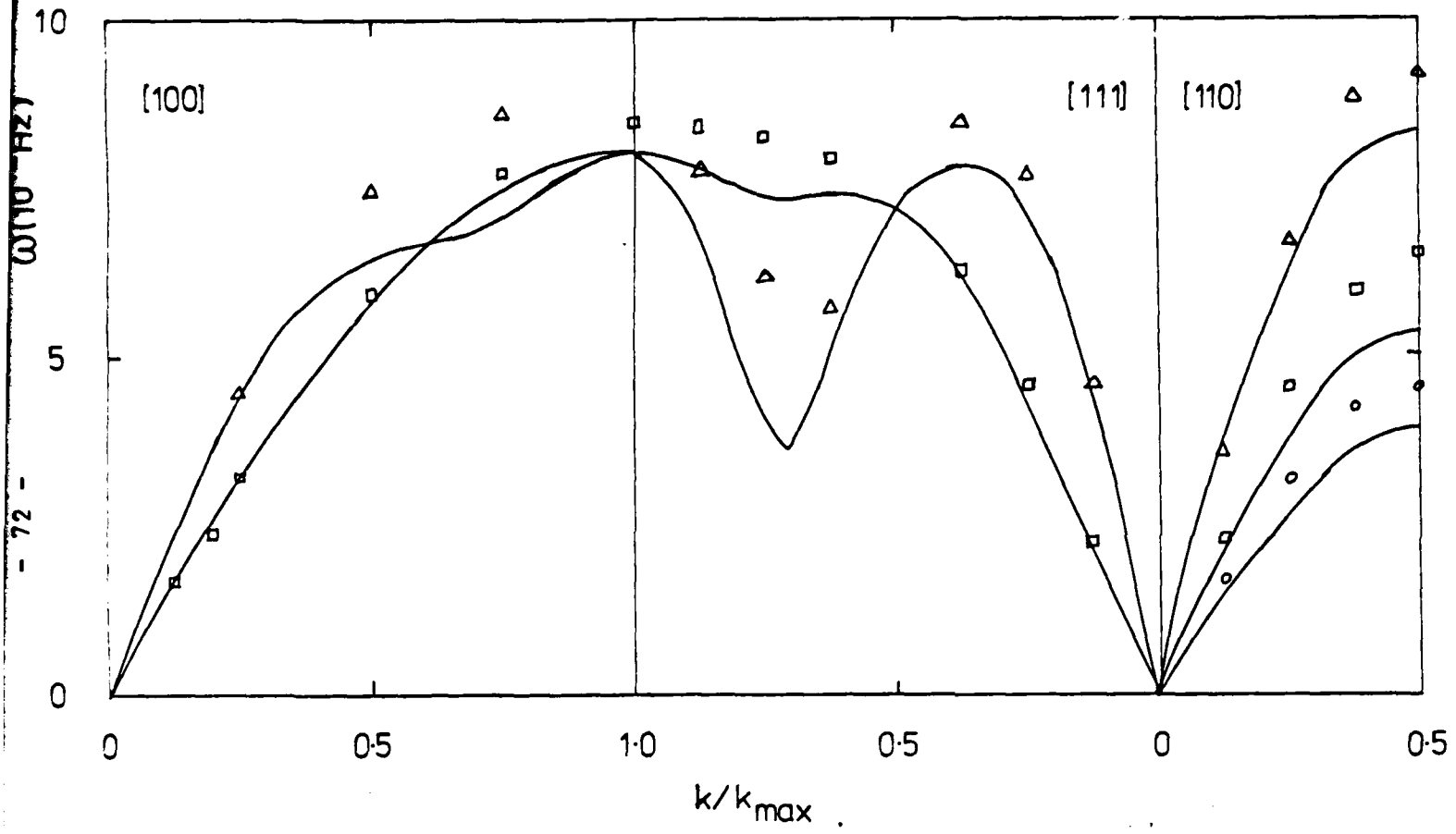

Figure 5.1

Calculated phonon dispersion curves of Fe with central pair potential only. Experimental results (Δ, □, ○) are from Brockhouse et al. (1967).

$$\phi_1(\underline{r}) = \frac{12800}{r^{16}} + \frac{4}{r^3} \cos(2.36r + 1.41) \exp(-0.05r)\text{eV} \qquad (5.11)$$

and is shown in figure 5.2. In calculating the phonon frequencies, we have truncated the potential at 7Å.

The lack of knowledge about the bond electron-bond electron and bond electron-ion interactions requires us to take an empirical approach in incorporating the bond charges into the formulation of the total energy.

Since, in the calculation of the elastic constants and of the phonon frequencies, we require only the first and second derivatives of the interacting potentials at the lattice and bond centre sites, we have treated them as parameters.

If the bond charges are small compared to the ionic charges, it follows that ϕ_2 will be larger than ϕ_3 in magnitude. The presence of the nearly free electron distribution in the solid ensures this to be the case and so to reduce the number of parameters we have neglected ϕ_3 from the expression for the total energy given in equation (5.3). Further, since ϕ_2 decays with distance, we only work to the first contributing set of parameters.

From equations (5.5) to (5.10) we find that the first contributing interactions to the phonon frequencies arises from that of the bond electron arising from next nearest neighbour bonding, which we have found to be greater than nearest neighbour bonding.

Hence, defining

$$K_1 = \left.\frac{d\phi_2(r)}{dr}\right|_{r = a/\sqrt{2}} \qquad (5.12)$$

and

$$K_2 = \left.\frac{d^2\phi_2(r)}{dr^2}\right|_{r = a/\sqrt{2}} \qquad (5.13)$$

where a is the cubic spacing, we find that the elastic constants are given by the equations

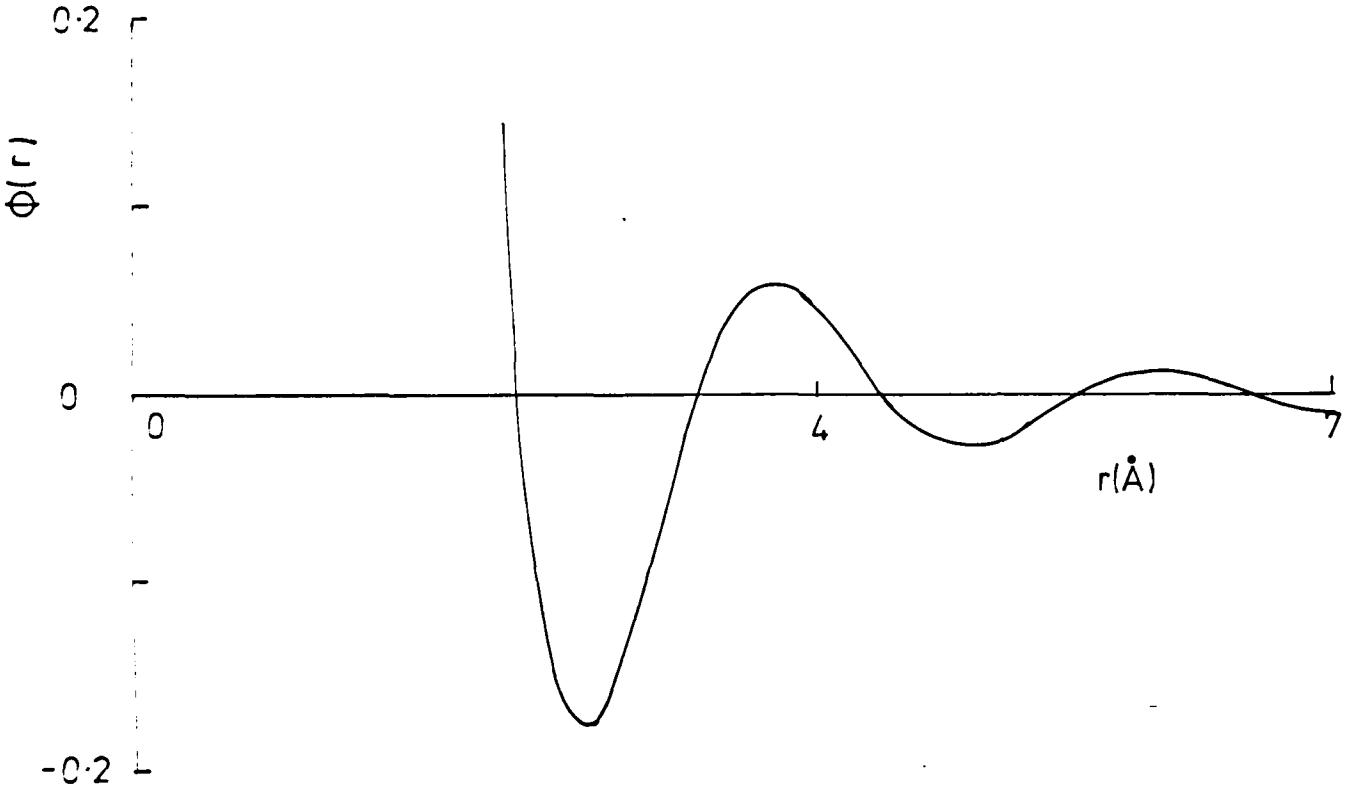

Figure 5.2

Central pair potential for Fe used to calculate phonon dispersion curves shown in Figure 5.1.

$$C_1 = \sum_s \psi_s' (x^s)^2 + 2\sqrt{2}K_1/a^2 + \epsilon_v' \qquad (5.14)$$

$$C_{11} = \sum_s \psi_1'' (x^s)^4 + K_2/(2a) + \epsilon_v'' - \epsilon_v' \qquad (5.15)$$

$$C_{22} = \sum_s \psi_1'' (x^s)^2(y^s)^2 + K_2/(\psi a) - K_1/(2\sqrt{2}a^2) + \epsilon_v'' + \epsilon_v' \qquad (5.16)$$

and

$$C_{44} = \sum_s \psi_1'' (x^s)^2(y^s)^2 + 3K_2/(8a) - K_1/(2\sqrt{2}a^2) - \epsilon_v'$$

The Cauchy discrepancy is then

$$C_{12} - C_{44} = - K_2/(8a) + \epsilon_v'' + 2\epsilon_v' \qquad (5.18)$$

We have calculated the phonon frequencies of Fe using equations (5.10) and (2.29) in the three main symmetry directions. The parameters K_1 and K_2 were varied until the experimentally determined dispersion curves were well reproduced. The parameter d in the volume dependent energy was chosen so that the Cauchy discrepancy remained positive. In figure 5.3 (a) we have plotted the dispersion curves for the best values of K_1, K_2 and d, and in figure 5.3 (b) the dispersion curves calculated with K_1 and K_2 equal to zero are shown. A comparison of the two figures shows the effect of introducing the bond charges, From figure 5.3.(a) we see the agreement with experiment is very good in the (110) direction and for small k in the (100) and (111) directions.

However, near the zone boundary in the (100) and (111) directions, the agreement is less satisfactory. Also we find a crossing of the longitudinal and transverse branches in the (100) direction, which is not observed experimentally. The crossing exists even with central forces alone and hence it appears to be an artifact of the central pair potential that we have used. A variation of the parameters does remove the crossing, but at the expense of agreement in the other directions.

We have also calculated the second order elastic cons-

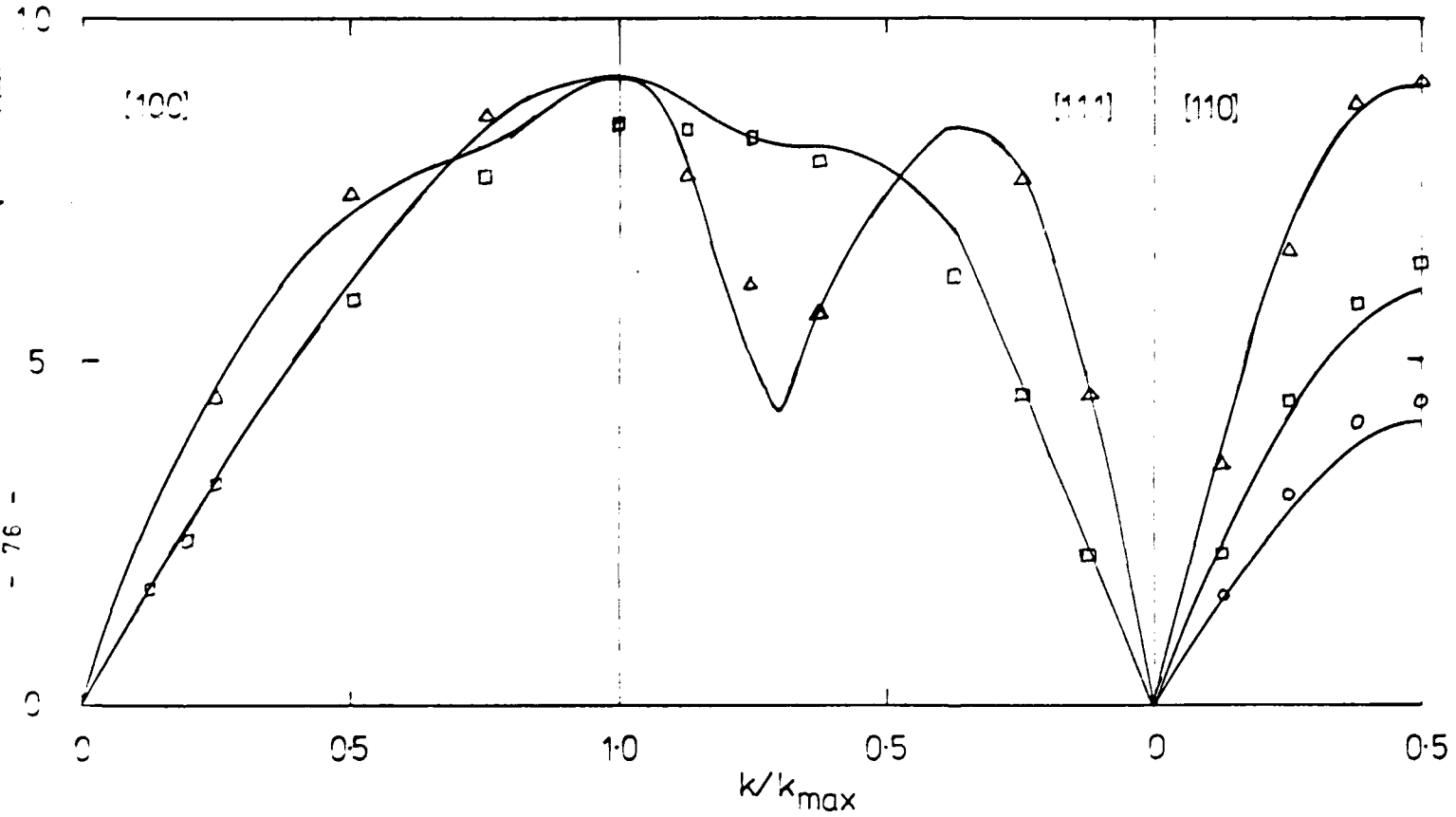

Figure 5.3 (a)

Phonon dispersion curve of Fe with angularity included.

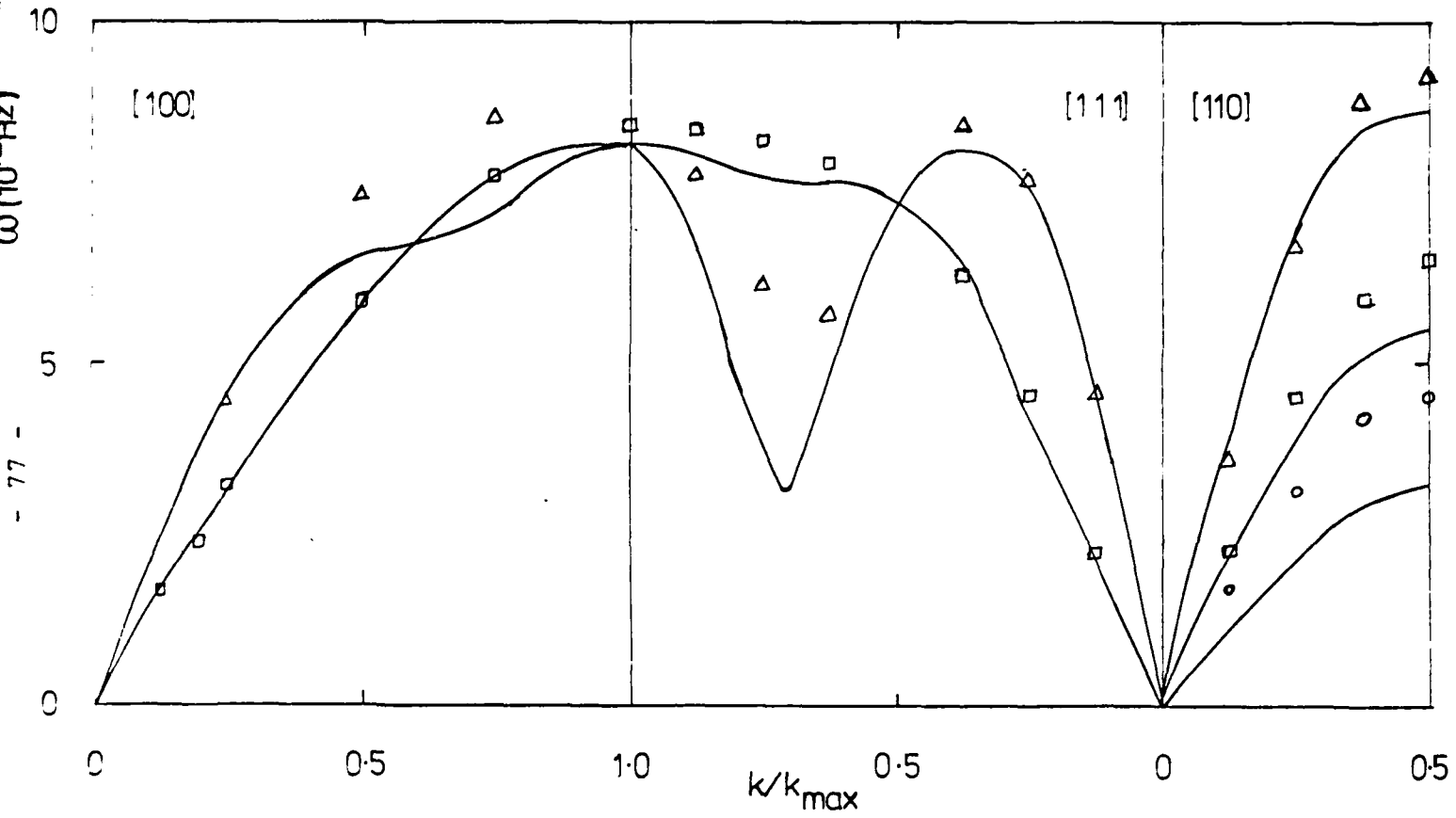

Figure 5.3 (b)

Phonon dispersion curves of Fe with K_1 and K_2 equal to zero.

tants with and without the angular contributions. From equation (5.18) it is clear that the angular interaction gives a negative contribution to the Cauchy discrepancy. The values of the parameters together with the elastic constants are tabulated in table 5.1.

§5.4 Discussion

As mentioned in Chapter 3, unlike in the f.c.c. metals, the experimentally determined phonon dispersion curves of the b.c.c. transition metals bear little resemblance to those of the b.c.c. simple metals. From our calculation of the phonon dispersion curves of Fe, we find that positive values of K_1 and K_2 lead to an increase in all the $\omega(\underline{k})$ at the zone boundaries and at the trough region of the $[1\bar{1}1]$ longitudinal branch. In contrast, the effect of $E_v(V)$ is to increase the frequencies of the longitudinal branches whilst decreasing those of the transverse modes. It also deepens the trough in the $[1\bar{1}1]$ longitudinal mode. Hence, the introduction of the bond charges provides an explanation of the different phonon dispersion relations observed in the b.c.c. transition metals. Chen and Brockhouse (1964), Shaw and Muhlestein (1971), Brockhouse et al (1967), Powell et al (1968) and Collela and Batterman (1970).

From equations (5.15) to (5.18), we see that the inclusion of the angular forces also provides the possibility of a negative Cauchy discrepancy. A positive or negative value of K_2, from equation (5.18) decreases or enhances respectively the Cauchy discrepancy. Hence, from the experimentally observed elastic constants, it would appear that in Fe, and to a greater extent in Cr, K_2 is positive whereas, it is negative in the other b.c.c. transition metals. This is consistent with our model. Since K_2 is the second derivative of the bond electron-ion potential, that is in all probability oscillatory, at distance $a/\sqrt{2}$, its values and sign depends on the lattice spacing, a. Thus, as Fe and Cr have lattice spacings of less than 3Å and the other b.c.c. transition metals have lattice spacings greater than 3Å, a change in sign in the second derivative is clearly possible if the wavelength of the oscillatory potential is of the

TABLE 5.1

The parameters used in the calculation of the phonon frequencies of Fe and the second order elastic constants.

$K_1 = 0.1875 \quad eV/\mathring{A}$

$K_2 = 0.0625 \quad eV/\mathring{A}^2$

Volume dependent Energy density = $0.036 \; eV/\mathring{A}^3$

$C_{ij}(10^{10} N/m^2)$	Expt. (a)	$E_v(V)$ = $K_1=K_2=0$	$K_1=K_2=0$ with angularity
C_{11}	23.3	27.85	31.16	31.34
C_{12}	13.6	13.19	14.79	14.75
C_{44}	11.8	13.19	14.15	14.15

(a) Gschneider (1964).

order of that of the central ion-ion pair potential. Hence, this model provides the facility of calculating a negative Cauchy discrepancy in Cr.

From our calculation of Fe, it is clear that a good pair potential is required before the effects of the angularity in the charge distribution can be studied. Figure 5.1 shows that the central ion-ion pair potential that we have extracted from the liquid state, although fairly good in reproducing the experimentally determined phonon dispersion curves of Fe, introduces a crossing of the longitudinal and transverse modes in the [100] direction. Although this crossing is shifted closer to the zone boundary on the introduction of the bond charges, its persistence leads us to believe that the central ion-ion pair potential that we have constructed may have to be further refined. However, it is interesting to note that even in the simple metals Na (Woods et al. 1962) and K (Cowley and Woods 1966) in which the force fields are central, this crossing is observed and thus we can safely assume that it is not a feature of the angularity in the force fields.

We have thus shown that the bond charge model described in §5.1 is very useful in understanding the phonon dispersion relations of the transition metals. Further, the general agreement with experiment leads us to conclude that next nearest neighbour bonding is more important than that of nearest neighbour bonding in the b.c.c. transition metals.

CHAPTER 6

Conclusion

The problem of determining the force field in a transition metal is clearly bound up with that of calculating the electron distribution. For example, in lattice dynamics within the adiabatic and harmonic approximations, the entire problem of the dynamical matrix and hence, the phonon dispersion relations hinges on calculating the change in the electron distribution as the ions are moved small distances from equilibrium.

Pair potential theory assumes that the localised charge distributions move rigidly with the ions as they vibrate. Though pair potentials afford the starting point of all the work presented here, the directional character of the d electrons in the transition metals demands corrections to this description of the force fields.

Of course, it is important in the d-band metals to recognise that the electrons in these materials have widely varying properties as one goes from itinerant s electrons to spatially localised d electrons, with, naturally enough, hybridized s-d electrons also playing an important role in the charge density and hence the force fields.

Thus, incorporating the unhybridized d electrons into the ionic charge distribution, the picture of a transition metal is that of a collection of ions situated at lattice sites and localised electron distributions arising from s-d hybrid overlaps immersed in a nearly free electron gas. In Chapter 2 we saw that the total energy of a crystal could be written as a sum of ion-ion pair interactions. In the above picture, the ions thus interact with each other directly, via the electron gas and via the localised electron distributions. We also saw that it is the last that gives rise to angularity in the ion-ion interactions.

To answer the first of the two questions posed in the

Introduction, we see that a central pair potential description would be valid only in those metals where the localised electron distributions are very small. From the arguments presented in Chapter 2 we saw that this would be best for those transition metals possessing the f.c.c. structure The usefulness of the central pair potential for Ni, extracted from the liquid structure data, in reproducing the experimentally determined phonon dispersion curves, suggests a starting point in the calculation of a central pair potential in solids. This view is confirmed by our calculations on Pt. The liquid structure calculated from the central pair potential, obtained by fitting the phonon dispersion curves, shows very good agreement with experiment. Thus, in Chapter 2 we showed that the concept of central forces is a useful one in the f.c.c. transition metals and the central pair potential in solids is directly related to that in the liquid state.

In an effort to obtain information about the angularity in the charge distribution and hence the force fields, we investigated the available X-ray scattering factor data on the transition metals in Chapter 3. By formulating the theory in terms of WF's. we showed that the charge distribution in the transition metals could be represented by bond charges situated mid-way between nearest and next nearest neighbours. The validity and usefulness of this formalism was demonstrated with a calculation on Be in Chapter 4.

Thus, with a useful representation of the charge density in the d-band metals we proceeded to construct a model by which the phonon frequencies of Fe were calculated. In this model, presented in Chapter 5, the force fields consisted of bond electron-bond electron and bond electron-ion interactions in addition to the effective ion-ion interaction present in the simple metals. Confidence in this approach has resulted from the application to the calculation of the phonon dispersion relations in Fe, where fairly satisfactory results were obtained. The ion-ion interaction in the transition metals has the same form as in the simple metals, i.e. given by equation (2.8). From our work we see that a semi-empirical way in which we can determine the

parameters is by appealing to the liquid structure factor data. The repulsivity, n, can be obtained from an analysis of melting and radiation damage data.

The volume dependent energy, $E_v(V)$ and the angular contribution can be represented in some form and the parameters determined by relating it closely to experimental data.

By perturbation theory, the bond electron interactions will also be oscillatory in nature. However, it is not clear whether it is correct to consider all the two body interactions separately. A more correct approach would be to treat all the electrons together in a mixed WF and plane wave formulation. However, from this first principles approach as formulated by Pick et al. (1970) and Hanke (1973), it is not easy to understand the nature of the force fields in real space.

Finally, we wish to make some comments about the accuracy of the potentials that have been constructed in this thesis. Though, as mentioned in §2.6 the parameters of the central pair interaction are accurate to better that 95%, it must be noted that we have assumed a particular form for the interaction. This form was motivated by that arising from the asymptotic form of the displaced charge around an ion in any electron gas, and is rigorously valid only at very large distances. We have in this work also not taken into account the changes in the potential due to density and pressure variations, although we recognised that the central pair potential in the liquid differs from that in the solid. From figure 2.2., we see that again the differences are only of the order of 5%. The aim of this work has, however, been to obtain practically useful representations of the force fields in the transition metals. The results which have been obtained by appealing to certain experimental data must be able to reproduce other quite different, experimental results before any claims of a true representation of the force fields in the transition metals can be made. For example, an important question for future work would be whether or not such force fields were useful in calcul-

ating vacancy and/or self interstitial energies in the transition metals. This problem, and more generally that of defect interactions, is of sufficient technological importance to warrant a fully study with the currently available force fields.

References

S.L. Altmann, C.A. Coulson and W. Hume-Rothery (1957), Proc. R. Soc. London Ser A 240, 145.

H.H. Anderson and P. Sigmund (1965), Risó-Report No. 103, (Danish AEC).

N.W. Ashcroft and D.C. Langreth (1967), Phys. Rev. 159, 500.

B.W. Batterman, D.R. Chipman and J.J. De Marco (1960), Phys. Rev. 122, 68.

C.M. Bertoni, O. Bisi, C. Calandra and F. Nizzoli (1975), J. Phys. F5, 419.

B.J. Birgeneau, J. Cordes, G. Dolling and A.D.B. Woods (1964), Phys. Rev. 136, A1359.

M. Born and H.S. Green (1946), Proc. Roy. Soc., A188, 10.

B.N. Brockhouse, H.E. Abou-Helal and E.D. Hallman (1967), Solid State Comm. 5, 211.

P.J. Brown (1972), Philos. Mag. 26, 1377.

P.J. Brown and W.H. Taylor (1969), Physics of Metals, ed. J.M. Ziman, (CUP) Vol. 1, 317.

J.F. Cannon (1974), J. Phys. Chem. Ref. Data 3, 781.

S.H. Chen and B.N. Brockhouse (1964), Solid State Comm. 2, 73.

F. Chikazumi (1979), Journ. Magnetism and Magnetic Material 10, 113.

R. Collela and B.W. Batterman (1970), Phys. Rev. B1, 3913.

C.S.G. Cousins and J.W. Martin (1978), J. Phys. F8, 2279.

R.A. Cowley and A.D.B. Woods (1966), Phys. Rev. 150, 487.

J. de Klerk (1959), Proc. Phys. Soc. London 73, 337.

J.J. De Marco and R.J. Weiss (1965), Phys. Rev. 137, A1869.

B.G. Dick, Jr. and A.W. Overhauser (1958), Phys. Rev. 112, 90.

B. Donovan (1952), Philos. Mag. 43, 868.

J.R. Drabble and J. Fendley (1967), J. Phys. Chem. Solids 28, 669.

D.H. Dutton, B.N. Brockhouse and A.P. Miller (1972), Can. J. Phys. 50, 2915.

W.E. Duncanson and C.A. Coulson (1944), Proc. Roy. Soc. Edinb. A 62, 37.

F. Flores, N.H. March, Y. Ohmura and A.M. Stoneham (1979), J. Phys. Chem. Solids 40, 531.

K. Fuchs (1936), Proc. Roy. Soc. A153, 622.

J.B. Gibson, A.N. Goland, M. Milgram and G.H. Vineyard, (1966), Phys. Rev. 120, 1229.

K.A. Gschneider, Jr. (1964), Solid State Physics, H. Ehrenreich, F. Seitz and D. Turnbull, Eds. (Academic, New York) 16, 275.

W.R. Hanke, (1973), Phys. Rev. B8, 1585.

W.A. Harrison (1966), Pseudopotentials in the Theory of Metals, Benjamin, New York.

W.A. Harrison, (1969), Phys. Rev. 181, 1036

Y. Hiki and A.V. Granato (1966), Phys. Rev. 144, 411.

P.S. Ho (1970), Interatomic Potentials and Simulation of Lattice Defects, eds. P.C. Gehlen, J.R. Beeler, Jr, and R.I. Jaffee, Plenum, New York, 321, especially discussion.

W.G. Hoover and M. Ross (1971), Contemp. Phys. 12, 339.

S. Hosoya and T. Yamagishi (1966), J. Phys. Soc. Japan 21, 2638.

M.J. Huijben and W. van der Lugt (1979), Acta Crystallogr. A35, 431.

H.B. Huntington (1953), Phys. Rev. 91, 1092

O. Inkinen and P. Sourtti (1964), Ann. Acad. Scient. Fenn. AVI, 147.

S.T. Inoue and J. Yamashita (1973), J. Phys. Soc. Jpn 35, 677.

M.D. Johnson, P. Hutchinson and N.H. March (1964), Proc. Roy. Soc. A282, 283.

M.W. Johnson, N.H. March, B. McCoy, S.K. Mitra, D.I. Page and R.C. Perrin, (1976),Philos. Mag. 33, 203.

J.E. Lennard-Jones (1924), Proc. Roy. Soc. A106, 441.

F.A. Lindemann (1910), Phys. Zeits. 11, 609.

P.-O. Lowdin (1956), Adv. in Phys. 5, 1.

J. Mahanty, D.D. Richardson and N.H. March (1976), J. Phys. C9, 3421.

J.W. Martin (1975), J. Phys. C8, 2837.

C.C. Matthai, P.J. Grout and N.H. March (1978a), Int. J. Quant. Chem. Symp. 12, 443.

C.C. Matthai, P.J. Grout and N.H. March (1978b) Phys. Lett. 68A, 351.

C.C. Matthai (1979), D. Phil Thesis, Oxford (unpublished).

H.J. McSkimmin and P. Andreatch, Jr. (1964), J. Appl. Phys. 35, 3312.

V.J. Minkiewicz, G. Shirane and R. Nathans (1967), Phys. Rev. 162, 528.

J. Moriarty (1972), Phys. Rev. B6, 1239.

T. Paakari and P. Suortti (1967), Acta Crystallogr. 22, 755.

R.M. Pick, M.H. Cohen and R.M. Martin (1970), Phys. Rev. B1, 910.

B.M. Powell, P. Martel and A.D.B. Woods (1968), Phys. Rev. 171, 727.

V.P.N. Sarma and P.J. Reddy (1979), Philos. Mag. 27, 769.

W.H. Shaw and L.D. Muhlestein (1971), Phys. Rev. B4, 969.

F. Simon (1937), Trans. Faraday Soc. 33, 65.

B. Stenhouse, P.J. Grout, N.H. March and J. Wenzel (1977), Philos. Mag. 36, 129.

J.F. Thomas, Jr. (1968), Phys. Rev. 175, 955.

B.B. Tripathi and S. Nand (1979), Phys. Lett. 70A, 241.

J.C. Upadhyaya (1978), Phys. Rev. B18, 2961.

P. Vajda (1977), Rev. Mod. Phys. 49, 481.

L. Verlet (1967), Phys. Rev. 159, 98.

Y. Waseda and M. Ohtani (1975a), Z. Physik B21, 229.

Y. Waseda and M. Ohtani (1975b). Z. Naturforsh. 30a, 485.

R.J. Weiss (1968), X-ray Determination of Electron Distributions, North-Holland.

A.D.B. Woods, B.N. Brockhouse, R.H. March, A.T. Stewart and R. Bowers (1962), Phys. Rev. 128, 1112.

C.J. Wright, J. Howard and T.C. Waddington (1976), J. Chem. Phys. 64, 3897.

Y.W. Yang and P. Coppens (1978), Acta Crystallogr. A34, 61.


DATE
FILME
8